2009

Two-tank indirect thermal storage designs for solar parabolic trough power plants

Joseph E. Kopp
University of Nevada Las Vegas

TWO-TANK INDIRECT THERMAL STORAGE DESIGNS FOR SOLAR PARABOLIC TROUGH POWER PLANTS

By

Joseph E. Kopp

Bachelor of Arts in Physics
Lewis & Clark College
2004

A thesis submitted in partial fulfillment
of the requirements for the

Master of Science Degree in Mechanical Engineering
Howard R. Hughes College of Engineering
Department of Mechanical Engineering

Graduate College
University of Nevada, Las Vegas
August 2009

ABSTRACT

Two-Tank Indirect Thermal Storage Designs for Solar Parabolic Trough Power Plants

by

Joseph Kopp

Dr. Robert F. Boehm, Examination Committee Chair
Professor of Mechanical Engineering
University of Nevada, Las Vegas

The performance of a solar thermal parabolic trough plant with thermal storage is dependent upon the arrangement of the heat exchangers that ultimately transfer energy from the sun into steam. The steam is utilized in a traditional Rankine cycle power plant. The most commercially accepted thermal storage design is an indirect two-tank molten salt storage system where molten salt interacts with the solar field heat transfer fluid (HTF) through a heat exchanger. The molten salt remains in a closed loop with the HTF and the HTF is the heat source for steam generation. An alternate indirect two tank molten salt storage system was proposed where the molten salt was utilized as the heat source for steam generation. A quasi-steady state simulation code was written to analyze the key environmental inputs and operational parameters: solar radiation, solar field size, thermal storage system, heat exchangers, and power block. A base case with no thermal storage was modeled using design parameters from the SEGS VI plant and the effects of solar field size were analyzed. The two differing indirect two-tank molten salt storage designs were modeled and their solar field size and thermal storage capacity were treated as parameters. Results present three days of distinct weather conditions for Las

Vegas, Nevada. Annual and monthly electricity generation was analyzed and the results favor the thermal storage case with the solar field HTF interacting with steam. Additionally, the economic trade offs for the three arrangements and speculation of operating strategies that may favor the alternate storage design is discussed.

TABLE OF CONTENTS

LIST OF FIGURES

LIST OF TABLES

NOMENCLATURE

A_i , A_o	= Heat exchanger surface area [m²]
cp , cp_1 , cp_2	= Specific heat capacity [J/kgK]
D , D_o , D_i	= Diameter of tube inside shell and tube heat exchanger [m]
dT	= Incremental change in temperature [°C]
DNI	= Direct normal irradiance [W/m²]
ε , $\varepsilon_{decrease}$, ε_{ref}	= Isentropic efficiency
$EndLoss$	= Amount of sunlight reflected off the end of an SCA unit
η_{field}	= Thermal efficiency of the solar field
η_{HCE}	= Thermal efficiency of the heat collection element
h , h_i , h_o	= Fluid heat transfer coefficient [W/m²K]
h_{in} , h_{out} , h_{mix}	= Fluid enthalpy [J/kg]
IAM	= Incidence angle modifier
k	= Thermal conductivity [W/m²K]
L	= Length of heat exchanger tubes [m]
$M_{\tan k}$	= Mass [kg]
$\dot{m}$	= Mass flow rate [kg/s]
μ	= Dynamic viscosity [Pa s]
Nu	= Nusselt Number
P	= Pressure [bar]
Pr	= Prandtl number
$\dot{Q}_{abs}$	= Energy rate absorbed by solar field [W]
$\dot{Q}_{collected}$	= Heat rate collected by solar field [W]
$\dot{Q}_{pipe\_loss}$	= Heat loss rate in pipes through solar field to power block [W]
$\dot{Q}_{receiver\_loss}$	= Heat loss rate in heat collection element [W]
Q	= Energy [J]
R''_{fi} , R''_{fo}	= Fouling resistance inside heat exchanger [m²K/W]
Re_D	= Reynolds number
$RowShadow$	= Fraction of solar radiation not blocked by neighboring SCA units
$SFAvail$	= Fraction of year the solar field is in operation
T , $T_{\tan k}$	= Temperature [°C]
θ	= the elevation angle between the sun and zenith
UA	= Heat exchanger overall heat transfer coefficient [W/K]

Subscript Terms

i,o	= ‘i’ indicates within tube, ‘o’ indicates outside of tube
ref	= Value at reference/design conditions

ACKNOWLEDGEMENTS

I would like to thank Dr. Robert Boehm for the opportunity to work at the Center for Energy Research and for providing me with many tools for professional growth. I would also like to thank every one at the Solar Site, past and present, who have helped me along the way. Finally, I would like to thank my parents and siblings who are always there providing me with non-technical support.

CHAPTER 1

INTRODUCTION

Background

Concentrating solar thermal power for utility-scale electricity generation is experiencing unprecedented growth. The three major divisions within concentrating solar thermal power are parabolic troughs, solar towers, and dish Stirling technology. Parabolic trough power plants are considered to be the most commercially ready technology.

Groundwork for commercial parabolic trough power plants was developed by the Luz International Limited from 1984 to 1990. A total of nine solar plants, ranging from 30-80 megawatts electric (MWe) were constructed in California and continue to operate today. The sixth solar electric generating systems (SEGS) plant, SEGS VI, included in Figure 1, has become the focal point of published research on parabolic trough power plants. The design conditions for this study were based on information provided for the 35 MWe SEGS VI plant.

Figure 1: SEGS III to SEGS VII in Kramer Junction, California [1]

In 2007, Nevada Solar One, a 64 MWe parabolic trough power plant, began operations near Las Vegas, Nevada. Acciona Solar Power operates the plant, shown in Figure 2, and it was the first utility-scale parabolic trough power plant built in the new millennium. This plant has been operating well for the past two years.

Figure 2: Nevada Solar One [2]

Construction finished on Andasol 1, shown in Figure 3, in November 2008. This plant is designed with a molten salt storage system capable of 7 hours of full-capacity power production. This is the first commercial parabolic trough plant to implement a molten salt two tank storage system. Thermal storage was utilized in SEGS I but the storage medium was the synthetic oil solar field heat

transfer fluid, or HTF. Synthetic oils are no longer considered for a storage medium in part due to their higher cost [3].

Figure 3: Thermal storage tanks at Andasol 1 [4]

The future of parabolic trough technology is bright as there are over 1000 MW of plants under construction and even more have been announced [5]. Many of these plants claim thermal storage will be integrated into their plant design.

The principle advantages of thermal energy storage in a solar parabolic trough power plant are the ability to control the time and quantity of power production. Herrmann [6] asserts thermal storage can be applied for: buffering

during transient weather conditions, dispatchability, increased annual capacity factor, and more even distribution of electricity production. Thermal storage can provide the stability necessary for base load operation and it also can have the economic advantage to discharge surplus power during peak demand hours.

Additionally, the annual solar-to-electric efficiency can improve as a result of thermal storage. Price [7] showed that the improvements to turbine start-up, excess heat from the field, improved parasitic losses, and negligible energy loss from “below turbine minimum” outweigh the storage thermal losses and reduced power plant steam cycle efficiency due to storage.

Review of Plant Modeling

In 1995, Frank Lippke [8] published results from a model of the SEGS VI plant that used EASY simulation software. His work included reference design values for the power block and several equations he presented were utilized in the current study. One objective of his work was to examine how to optimize the HTF’s solar field outlet temperature and flow rate. His results suggest the highest allowed HTF temperature is optimum for a summer day; however during fall and winter conditions the superheating temperature should not greatly exceed the design value.

The Solar Advisor Model, SAM [9], is modeling software developed by the National Renewable Energy Laboratory. The publicly available source code is written in FORTRAN, is, and runs off software called TRNSYS. SAM is a work in progress and its current state does not represent a complete thermophysical

model of a solar parabolic trough power plant. As a result, it could not be used to perform the desired parametric studies. Among the benefits of this program, however, are rapid computations and calculations of levelized cost of energy.

TRNSYS has a large set of solar parabolic trough power plant components. The solar thermal electric component library, STEC, is organized by the international organization SolarPACES. A model of SEGS VI was available that utilized STEC components; however the complex model had convergence issues.

Numerous private parabolic trough power plant models exist, such as PCTrough™ by Solar Millennium, but they are not accessible in the public domain. Patnode [10] performed a detailed simulation of SEGS VI using Engineering Equation Solver, EES, and TRNSYS. Equations and design values presented by Patnode were also used utilized in this work.

A new solar parabolic trough power plant model was built for this study using Matlab™. The code reflects the design considerations of the 35 MWe SEGS VI plant, though modeling the precise performance of the plant was out of the scope of this project. Absolute precision was not necessary when the objective was to consider the behavioral differences of competing storage designs applied to the same solar field and weather conditions. The code was written to calculate the gross electrical power but not parasitic losses. For each power plant design the solar field size and the storage tank sizes were treated as parameters.

Data from the Typical Meteorological Year 3, TMY3, was utilized for local weather conditions. Component calculations were performed for a one second

interval to maintain scientific units. Values for power were calculated hourly. This model will allow smaller time increments than hourly values given by TMY3. Hourly energy totals were found with ease since the MW produced in one second integrated over an hour equal the accepted energy unit of mega-watt hours (MWh).

Solar Parabolic Trough Plant

The cornerstone of solar parabolic trough plant is the solar field. The solar field consists of parabolic trough collectors and piping. Parabolic trough collectors can be divided into two subsystems: the solar collection assembly (SCA) and the heat collection element (HCE).

A highly reflective material covers the parabolic surface area of the SCA. The SCA also includes the single-axis tracking equipment and support structure for the HCEs. Typically the SCA units are aligned along the North-South axis and track the sun from East to West. During operation, solar radiation is reflected from the SCA onto the parabolic trough's focal line, where the HCE resides.

The outer glass shell of the HCE receives approximately 75 times the amount of direct normal irradiation (DNI) as a non-concentrated surface. When radiation is transmitted through the glass shell it passes through a vacuum and arrives at the absorber tube. Vacuum conditions prevent conduction and convection heat losses from the absorber tube to the environment. The absorber tube's outer surface is covered in a ceramic metal (cermet) coating designed to minimize radiation losses in the infrared region of the electromagnetic spectrum.

The absorber tube conducts thermal energy to its inner surface and provides the heat source for the HTF flowing within the tube. The HTF receives heat from the inner surface through convection, conduction, and radiation.

The solar field depicted in Figure 4 heats the HTF (red line) that travels through piping to the power block. The flow is separated in the power block into two parallel heat exchanger elements: the steam train and the reheater.

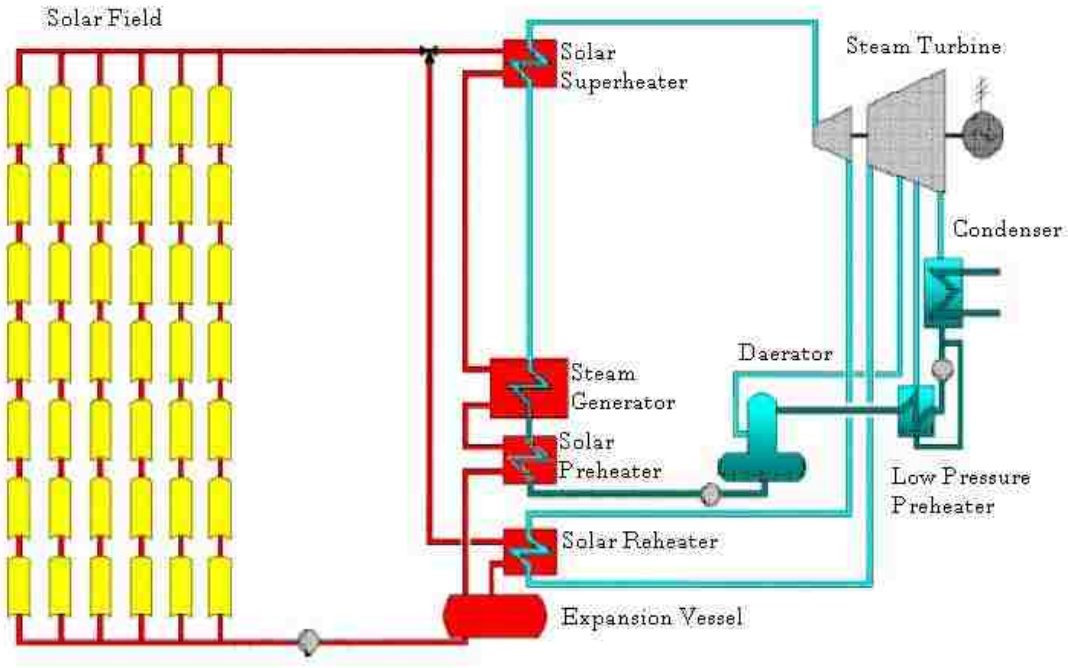

Figure 4: General solar parabolic trough plant design [11]

The steam train is a term used to describe the heat exchangers that heat the working fluid, highly pressurized water, from a compressed liquid state into a superheated vapor state. The preheater warms the working fluid from compressed liquid to saturated liquid. Water boils in the steam generator and exits as a saturated vapor. Due to the latent heat of evaporation the steam generator is the most energy intensive heat exchanger. The superheater utilizes the highest temperature HTF to heat the saturated vapor into superheated steam.

The superheated steam performs work on a high pressure turbine and typically loses enough heat to enter the saturation region. An abbreviated temperature-entropy (Ts) diagram for power cycle design conditions for SEGS VI [8] is shown in Figure 5. The design conditions illustrate the ideal case where the working fluid reaches the saturated vapor state. The reheater serves to superheat the steam a second time. The pressure of the steam exiting the reheater has been reduced and is utilized to perform work on a low pressure turbine. There are two high pressure turbine stages and five low pressure turbine stages for a total of seven turbine stages.

The quantity and size of each type of heat exchanger will vary given the size of a plant. Heat exchangers can only reach a functional length before the surface area demands require additional units. For modeling purposes a control volume approach eliminates the need for actual heat exchanger dimensions.

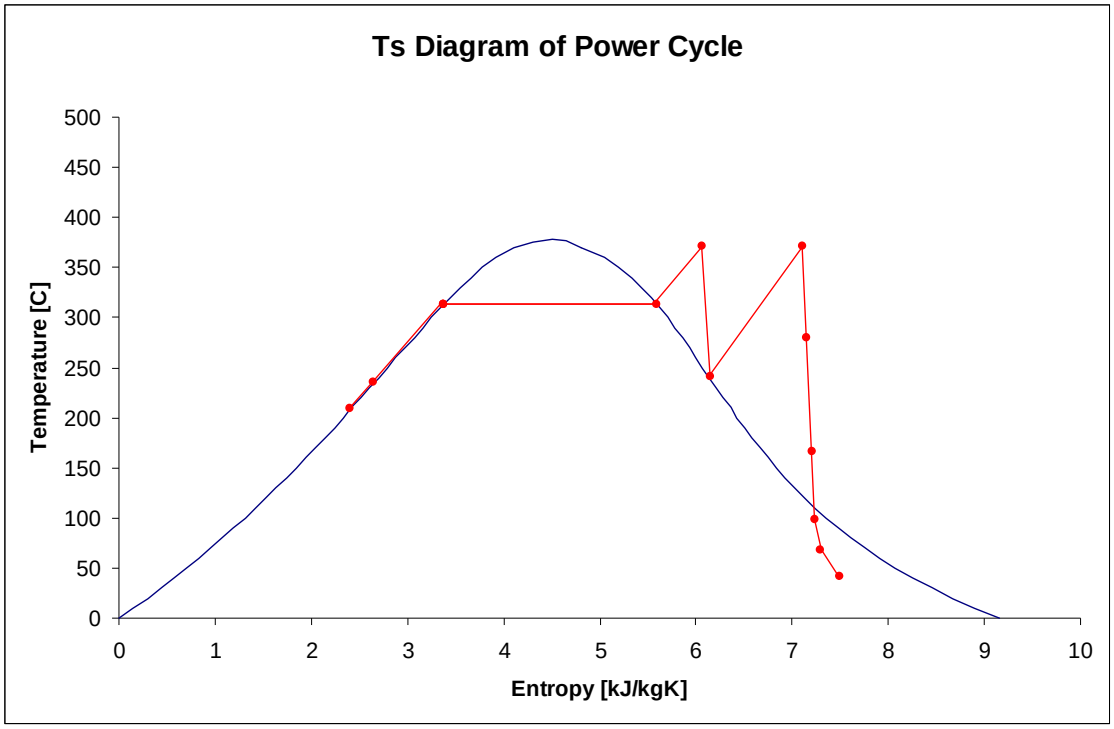

Figure 5: Abbreviated Ts Diagram for design points of SEGS VI Power Cycle

Steam exiting the low pressure turbine undergoes a phase change in the cooling process so water can be pumped to the preheater and the cycle can repeat. Cycle completion for the HTF includes passing through the expansion vessel, which among several functions, serves as a mixing unit.

The mass flow rate and HTF outlet temperature from the solar field are important values. Generally, a higher mass flow rate from the field will translate into a higher mass flow rate of steam but at the cost of lower temperature. The highest field outlet temperature can provide the highest steam enthalpy into the turbine but at a cost of lower water flow rate. It has been suggested by another

author that neither strategy displays a significant improvement in overall plant performance [10]. Some models treat both values as outputs while this model treats the HTF outlet temperature as a parameter. The operating strategy in this model was chosen to maximize outlet temperature since the highest quality of thermal storage is desirable.

The solar multiple is defined as the solar collector area divided by the solar collector area necessary for nominal power generation. The solar collector area necessary to generate nominal power is considered to be a fundamental design condition for a plant. The design condition may be chosen for a direct normal irradiation level (DNI) of 800 W/m^2 or the typical solar radiation value at noon on the spring equinox [3]. The design of SEGS VI was assumed have a solar multiple (SM) equal to one. A plant optimized at SM 1 has the potential to collect a surplus of solar energy under high solar radiation periods. The amount of surplus energy, however, does not justify the costs of implementing thermal storage. An increase in SM will increase the collector area in the solar field and will lead to more thermal energy available for storage. If solar energy cannot be collected or stored, parasitic losses are reduced by moving SCA units to stow and maintaining design flow rate conditions.

Storage Design Oil-Water: Synthetic Oil Steam Generation

Indirect two-tank thermal storage can be integrated into a parabolic trough plant, as shown in Figure 6. This is the most commercially ready thermal storage design and may be referred to as Storage Oil-Water because the synthetic oil

HTF is the heat source in steam generation. While actual operational schemes may be quite complex, the addition of thermal storage does not have to significantly affect the overall operating strategy.

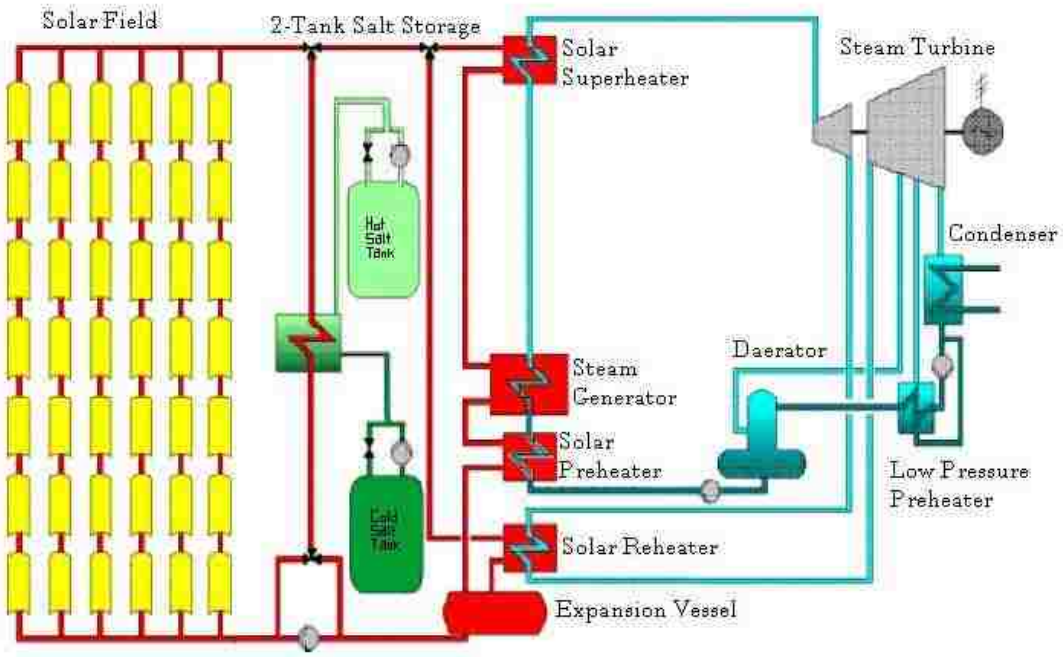

Figure 6: Plant design with thermal storage [11]

The basic operating strategy is to charge thermal storage when the HTF flow rate exceeds the design flow rate for steam generation. Surplus flow travels through the oil-to-salt shell and tube heat exchanger to charge molten salt then

exits to the expansion vessel. During charging, molten salt leaves the cold tank extracts heat from the HTF, and then enters the hot tank.

Ideally the design flow rate of HTF is maintained during operating hours so discharging from the hot tank should be performed to maintain the maximum HTF flow rate through the steam train and reheater. Discharging salt from the hot tank to reheat the HTF occurs in the same heat exchanger except flow is reversed. Salt is always maintained on the shell side of the heat exchangers [12].

The first law of thermodynamics requires a temperature drop across a heat exchanger. The temperature of the HTF heated by discharging salt will be lower than the HTF temperature directly from the solar field because the heat has passed through two heat exchangers and an associated heat loss inside the hot tank. This decrease in temperature will result in a decrease in power generation.

The required volume of molten salt is considered to be the volume required to completely fill one tank. Consequently, if one tank is completely filled the other tank is empty. This is a simplification of the actual system, where a minimum volume of salt must be maintained within each tank [13]. When fully charged all the molten salt resides in the hot salt tank at maximum temperature of 386 °C. The design temperature of the cold salt tank is 293°C. The tanks are considered to be fully mixed thermally and have a heat loss correlation based on surface area of tank.

The oil-to-salt heat exchanger must be sized for the discharging capacity of the HTF at the design flow rate for steam generation. Therefore the size of the

heat exchangers must be optimized to transfer heat to the design HTF flow rate. If a solar field was designed for 800 W/m^2, then a solar multiple of 1.6 with DNI of 1,000 W/m^2 would provide double the HTF design flow rate. For any larger solar multiple, the oil-to-salt heat exchanger area must increase and subsequently its cost will increase.

To charge the HTF, the necessary flow rate is withdrawn from the expansion vessel and is mixed with HTF flow from the solar field, if there is any. If there is not enough heat in storage to bring the mass flow rate up to design flow, but enough hot molten salt to generate the minimum amount of power, the hot molten salt is discharged completely. Four MWe was the minimum amount of power assumed necessary for electricity generation. This corresponded to an oil mass flow rate of 40 kg/s. If the HTF flow rate could not reach 40 kg/s, even after thermal storage discharge, the hot salt would dwell in the hot tank and power would not be generated.

Storage Salt-Water: Molten Salt Steam Generation

The indirect two-tank molten salt storage proposed in Figure 7 is referred to as Storage Salt-Water. This is because molten salt is the heat transfer fluid in the steam train and reheater. The synthetic oil is contained in a closed loop around the solar field and the oil-salt heat exchangers. Although not illustrated, an expansion vessel will still be needed for the solar field.

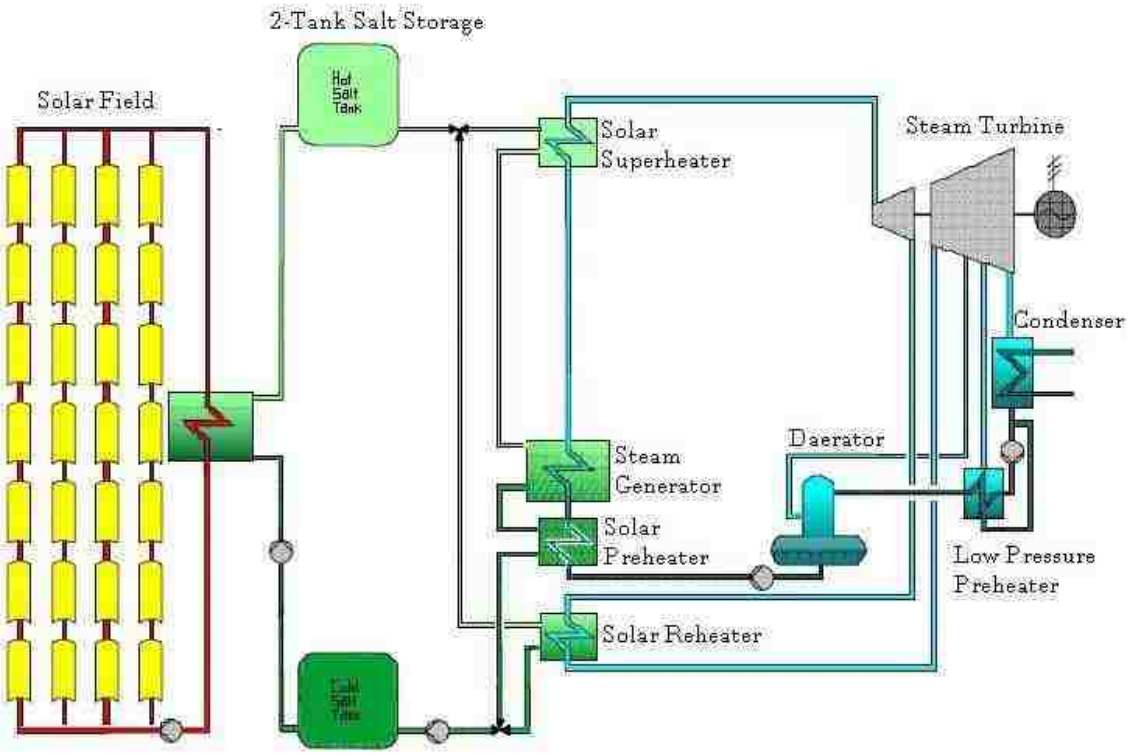

Figure 7: Storage Salt-Water design for indirect two tank thermal storage [11]

A significant difference between thermal storage plant designs is the number of heat exchangers encountered before transferring heat to the working fluid. No additional heat exchangers are required between the HTF and the working fluid during normal operating conditions for Storage Oil-Water. However, when heat is needed from storage, two additional heat exchangers are utilized. Heat is first transferred from oil to salt, then from salt back to oil, and finally from oil to the

working fluid. The Storage Salt-Water design utilizes two heat exchangers between the synthetic oil and the working fluid for all operations.

Storage Salt-Water requires a larger oil-salt heat exchanger area than the Storage Oil-Water case because all of the solar field HTF flow rate must transfer heat to the salt. While the heat exchanger area for Storage Oil-Water does not have to increase until SM 1.6, any increase in solar multiple for Storage Salt-Water will result in a larger oil-salt heat exchanger area. Based on the cost of oil-salt heat exchangers, Storage Oil-Water is heavily favored.

Integration of thermal energy storage decreases a plant's efficiency for the time period of thermal discharging. This is due to inevitable heat transfer losses to charge the thermal storage medium and also to discharge it. Molten salt is a leading medium for thermal storage and there is discussion it may be circulated through the solar field [14], thus reducing thermal losses through heat exchange.

The description of the molten salt steam generation is also crucial to the analysis of the Storage Salt-Water design. The behavior of molten salt as a heat transfer fluid is discussed in Chapter 2 and its design values compared to oil-water heat exchanger design values are presented in Chapter 3.

CHAPTER 2

HEAT TRANSFER RELATIONS

Solar Field Heat Transfer Fluid

The synthetic oil used as the solar field heat transfer fluid is a eutectic mixture of diphenyl oxide and biphenyl. Two commercial names for this product are Therminol VP-1™ and Dithers A™. It is stable up to 399 °C. The thermal properties of this mixture were selected from the SAM [9] source code and equations 1-4 describe them as functions of temperature. Included also as equation 5 is a relationship for temperature as a function of enthalpy.

Therminol VP-1™:

$$cp(T) = 1000 \cdot (1.509 + 0.002496 \cdot T + 0.0000007888 \cdot T^2) \quad [\text{J/kg/K}] \tag{1}$$

$$k(T) = 0.1381 - 0.00008708 \cdot T - 0.0000001729 \cdot T^2 \quad [\text{W/m/K}] \tag{2}$$

$$\mu(T) = 0.001 \cdot (10^{0.8703} \cdot T^{(0.2877 + Log(T^{-0.3638}))}) \quad [\text{Pa s}] \tag{3}$$

$$h(T) = 1000 \cdot (-18.34 + 1.498 \cdot T + 0.001377 \cdot T^2) \quad [\text{J/kg}] \tag{4}$$

$$T(h) = -0.000000000158 \cdot h^2 + 0.0006072 \cdot h + 13.37 \quad [\text{°C}] \tag{5}$$

Nitrate Salt

The molten salt chosen was a nitrate salt that is composed of 60% KNO_3 and 40% $NaNO_3$. Thermal properties for solar salt were found in SAM [9] and listed in equations 6-9. Among the benefits of the nitrate salt is its stability up around 600 °C. However, a disadvantage is its high melting point; Schulte-Fischedick [13] report that local solidification can occur at 239 °C.

Nitrate Salt:

$$cp(T) = 1443 + 0.172 \cdot T \quad [\text{J/kg/K}] \tag{6}$$

$$k(T) = 0.443 + 0.00019 \cdot T \quad [\text{W/m/K}] \tag{7}$$

$$\mu(T) = 0.001 \cdot (22.714 - 0.12 \cdot T + 0.0002281 \cdot T^2 - 0.0000001474 \cdot T^3) \quad [\text{Pa s}] \tag{8}$$

$$T(h) = 0.001 \cdot (22.714 - 0.12 \cdot T + 0.0002881 \cdot T^2 - 0.0000001474 \cdot T^3) \quad [\text{°C}] \tag{9}$$

The temperature of the cold tank is of concern because long periods without charging may lead to freezing conditions. Freezing is a distinct possibility if the salt is not heated by auxiliary heaters and a study showed the cold tank dropped from 293 °C to 239 °C in 50 days (without auxiliary heating) [13]. For a plant with a solar multiple close to one, there will be concerns of salt solidification in the winter months, when the flow rate of the field does not exceed design conditions. Freezing would not occur in the normal operations of the Storage Salt-Water case.

Despite freezing concerns, nitrate salt has been proven reliable and Relloso [4] states it was chosen as the storage media for Andasol 1. Auxiliary heaters were not included in this analysis, and the salt was allowed to drop below the freezing point (phase change was neglected). During charging the HTF had to supply additional heat to overcome the lower temperatures. This thermal energy requirement can be related to an internal parasitic loss.

Nitrate salt has a lower heat capacity than Therminol VP-1™ as shown in Figure 8. This is particularly important in the development of the molten salt steam train because it determines how much heat can be provided to each heat exchanger stage. In particular, the steam generator requires a larger temperature difference of molten salt. It is also important in the development of the oil-salt heat exchangers, as the salt flow rate must be higher than the oil flow rate to match the heat exchanged. Higher mass flow rate also represents higher pumping power losses. Pumping power losses are further augmented by nitrate salt's higher viscosity.

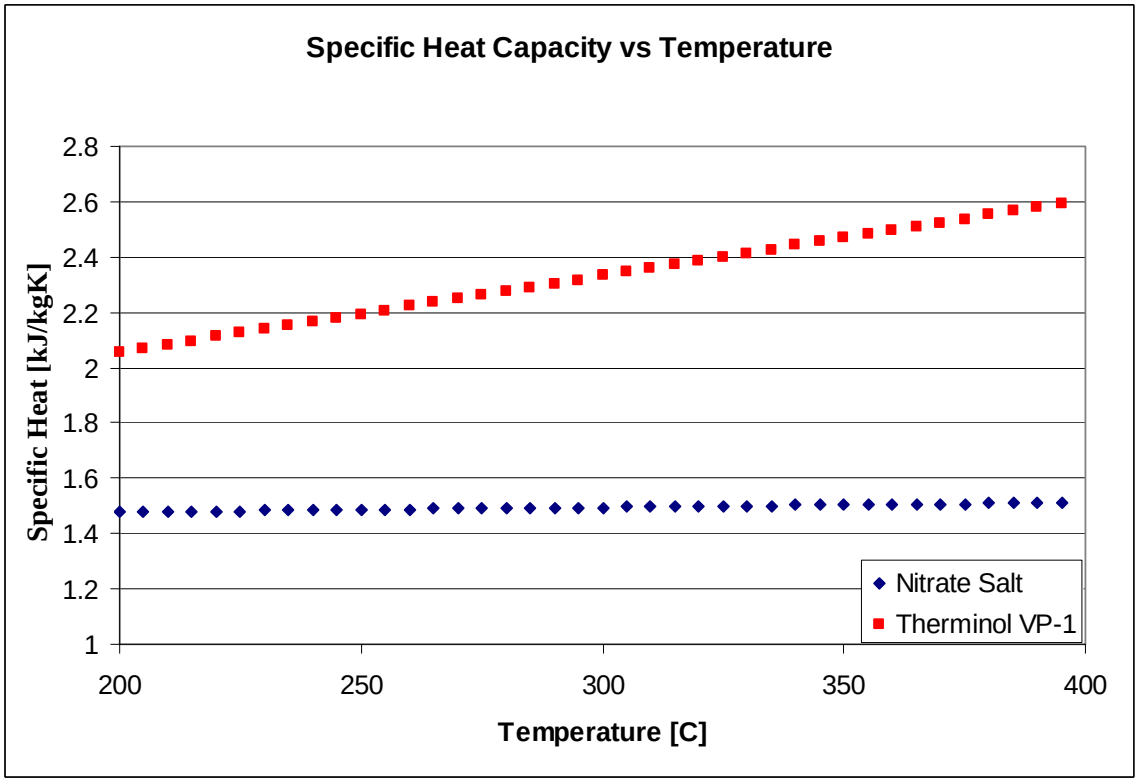

Figure 8: Specific heat of nitrate salt and Therminol VP-1™

Overall Heat Transfer Coefficient

The thermal properties of the two heat transfer fluids are further analyzed by their capabilities of transferring heat. The overall heat transfer coefficient applicable to shell and tube heat exchangers is determined by

$$\frac{1}{UA} = \frac{1}{h_i A_i} + \frac{R''_{fi}}{A_i} + \frac{\ln D_o / D_i}{2\pi kL} + \frac{R''_{fo}}{A_o} + \frac{1}{h_o A_o}, \tag{10}$$

from Incropera and Dewitt [15]. UA can be found for design conditions, however with an energy source as variable as the sun, off-design conditions occur often.

According to solar literature, the approximation for modeling the UA during off-design conditions is

$$\frac{UA}{UA_{ref}} = \left(\frac{\dot{m}}{\dot{m}_{ref}} \right)^{0.8} , \tag{11}$$

where the mass flow rate has been determined to be the dominant variable in UA. Patnode [10] provides a thorough derivation of this term and certain aspects are highlighted here. By neglecting the thermal resistance through the metal tubes and the resistance due to fouling is negligible, equation (10) becomes

$$\frac{1}{UA} = \frac{1}{h_i A_i} + \frac{1}{h_o A_o} . \tag{12}$$

Equation (12) implies that the behavior of UA is dominated by convective heat transfer. The contact surface area for each fluid and the heat transfer coefficient of the fluids on the inside and the outside of the tubes are the only values considered. Surface area will not change during off-design conditions so further a relative UA approximation can be performed by

$$\frac{1}{UA} \propto \frac{1}{h_i} + \frac{1}{h_o} . \tag{13}$$

The heat transfer coefficient is defined as

$$h = \frac{Nu \cdot k}{D} \tag{14}$$

where the Nusselt number for fully developed (hydrodynamically and thermally) turbulent flow in smooth circular tubes is

$$Nu_D = 0.023 \cdot \mathrm{Re}_D^{0.8} \cdot \mathrm{Pr}^n \quad . \tag{15}$$

For a cooling fluid where *n* = 0.3 and for a heating fluid *n* = 0.4. The Reynolds number is solved by

$$\mathrm{Re}_D = \frac{4 \cdot \dot{m}}{\pi \cdot D \cdot \mu}, \tag{16}$$

and the Prandtl number in equation (15) is

$$\mathrm{Pr} = \frac{\mu \cdot cp}{k} \quad . \tag{17}$$

Solving the Nusselt number for the heating fluid (n=3) gives

$$Nu_D = 0.023 \cdot \mathrm{Re}_D^{0.8} \cdot \mathrm{Pr}^{0.3} = 0.023 \cdot \left(\frac{4 \cdot \dot{m}}{\pi \cdot D \cdot \mu} \right)^{0.8} \cdot \left(\frac{\mu \cdot cp}{k} \right)^{0.3}. \tag{18}$$

After incorporation of all the terms the heat transfer coefficient becomes

$$h = \frac{0.023 \cdot \left(\frac{4 \cdot \dot{m}}{\pi \cdot D \cdot \mu} \right)^{0.8} \cdot \left(\frac{\mu \cdot cp}{k} \right)^{0.3} \cdot k}{D} \quad . \tag{19}$$

Once the physical dimensions of a heat exchanger have been established, *h* will only vary based on fluctuations in the mass flow rate and the temperature. This is shown by

$$h \propto \frac{\dot{m}^{0.8} \cdot cp(T)^{0.3} \cdot k(T)^{0.7}}{\mu(T)^{0.5}} \quad . \tag{20}$$

On a per kilogram basis Figure 9 shows the heat transfer coefficient's temperature dependence. The y-axis value is the product of the thermal

properties that are a function of temperature. The current operating temperature of parabolic trough plants is below 400 °C due to the stability of the HTF. This happens to be near the point of intersection where nitrate salt performs better than Therminol VP-1™.

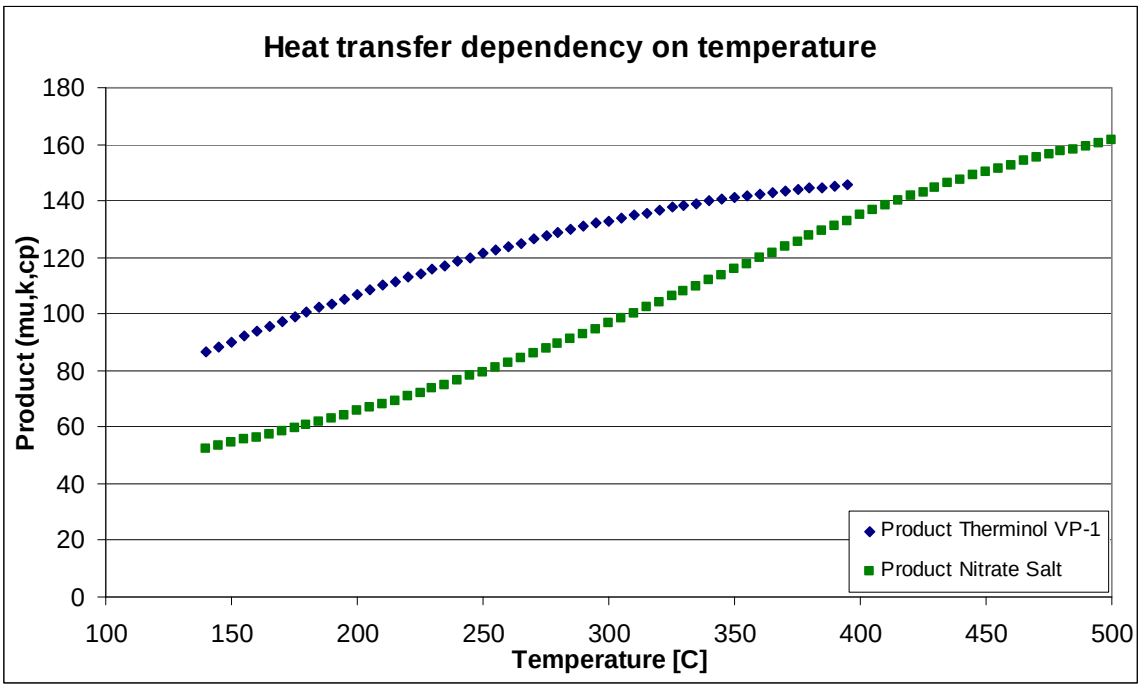

Figure 9: Heat transfer dependency on temperature per kg of fluid

Changes in the mass flow rate contribute significantly more to the heat transfer coefficient. Figure 10 illustrates the h values for salt and oil at their design flow rates. Nitrate salt is much larger due to the much higher flow rate, a result of its lower specific heat. The mass flow rate approximation is a good first

order perturbation for the off-design conditions of the overall heat transfer coefficient.

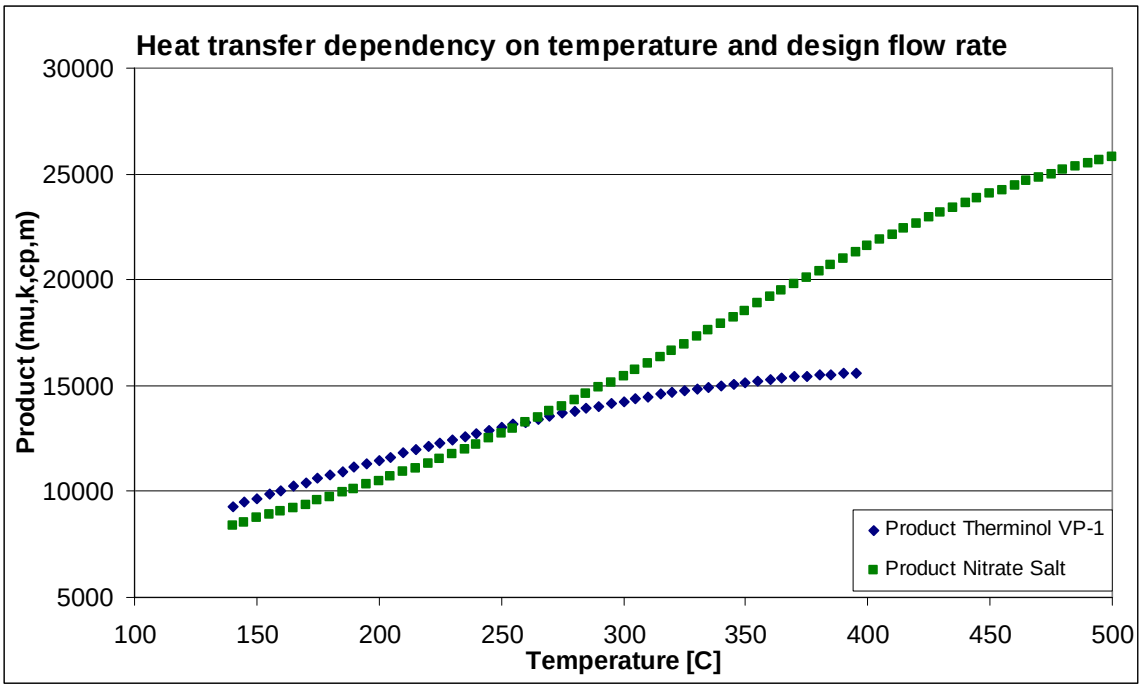

Figure 10: Heat transfer coefficients as products of variable components

If the heat transfer coefficient increases for a fluid then the overall heat transfer coefficient, U will become larger. Assuming identical UA values for the two fluids in a specific heat exchanger, a higher U value for one fluid implies a smaller area.

CHAPTER 3

MODEL COMPONENTS

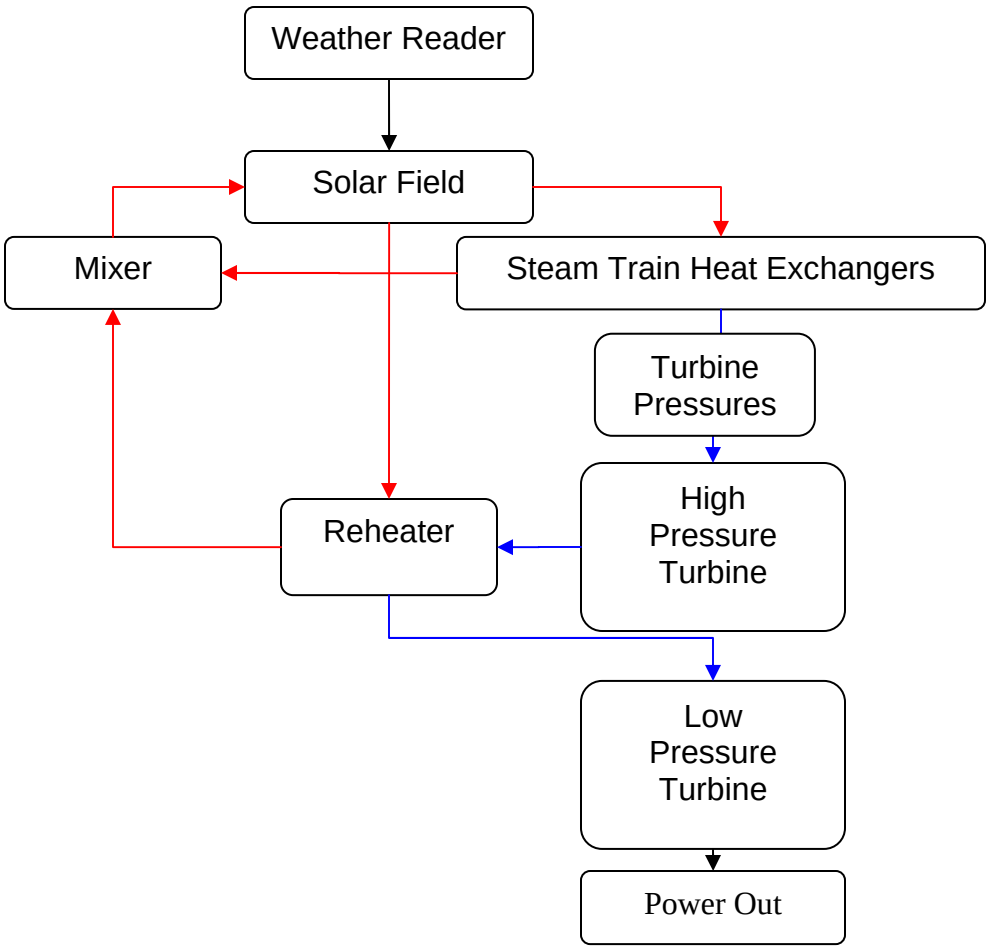

Figure 11: Flow chart for power plant components

Weather Reader and Solar Field

The Weather Reader component, shown in Figure 11, is called first to process weather conditions. Duffie & Beckman [16] describe the geometry of

tracking and sun angles based on local coordinates and Patnode [10] explicitly solves them for a parabolic trough plant. Values were calculated for Las Vegas, Nevada:

Longitude: - 115.08°

Latitude: 36.06 °N.

SCA length, spacing, focal length, and HCE values were used from Patnode [10]. A solar field row is formed by a series of 4 SCA units and the heat transfer fluid temperature increases incrementally over each SCA. Two rows are connected in series to form a loop in the solar field. Increases in solar multiple were calculated by increasing the number of loops in the solar field.

The total heat absorbed from the solar field is found by the calculation

$$\dot{Q}_{abs} = DNI \cdot \cos(\theta) \cdot IAM \cdot RowShadow \cdot EndLoss \cdot \eta_{field} \cdot \eta_{HCE} \cdot SFAvail \qquad (21)$$

The absorber tubes and HTF are hundreds of degrees Celsius above ambient weather conditions and thermal losses are significant. The amount of energy that can be actually be transferred from the solar field is called $\dot{Q}_{collected}$ and is found by

$$\dot{Q}_{collected} = \dot{Q}_{abs} - \dot{Q}_{pipe\_loss} - \dot{Q}_{receiver\_loss} \qquad (22)$$

The outlet temperature of the solar field, T_{out}, was assumed to be fixed at 390.56 °C. Inlet temperature, T_{in}, varied based on the last iteration and the mass flow rate was solved;

$$\dot{m} = \frac{\dot{Q}_{collected}}{c_p (T_{out} - T_{in})} \ . \qquad (23)$$

Further details on the solar field can be found in the Matlab™ code in Appendix A.

Heat Exchangers

A total of 10 distinct counter-flow shell and tube heat exchangers were characterized and simulated in the three models. The method for solving the unknowns in each heat exchanger differed depending on its position in the cycle. With the exception of the preheater, every heat exchanger required solving the heat transfer rate according to an energy balance and the effectiveness-NTU method. The preheater calculation was simplified to only require an energy balance.

The energy balance performed across the heat exchanger was solved using

$$\dot{m}_1 \cdot cp_1 \cdot \Delta T_1 = \dot{m}_2 \cdot cp_2 \cdot \Delta T_2 . \quad (24)$$

Patnode [10] found inaccuracies by assuming an adiabatic heat exchanger model. Heat loss through the heat exchangers was examined from adiabatic to 3% heat loss. At nominal power generation 3% heat loss in the heat exchangers led to a 1 MW difference in power generation. Three percent heat loss was chosen for all heat exchangers.

Design conditions for each heat exchanger not specified by the SEGS VI design were established and an overall heat transfer coefficient, UA, was derived to provide the necessary heat transfer. For each individual fluid, an energy balance was used where

$$Q = \dot{m} \cdot cp \cdot \Delta T \,, \tag{25}$$

and a mass balances for each fluid was

$$\dot{m}_{in} = \dot{m}_{out} \,. \tag{26}$$

Once the heat transfer was determined, the design UA was solved by

$$UA = \frac{Q}{\Delta T_{lm}} \,. \tag{27}$$

The log mean temperature difference, ΔT_{lm}, for a heat exchanger [17] is expressed as

$$\Delta T_{lm} = (\Delta T_I) - (\Delta T_{II}) / \ln(\Delta T_I / \Delta T_{II}) \,, \tag{28}$$

where for counterflow

$$\Delta T_I = T_{h,i} - T_{c,i} \tag{29}$$

and

$$\Delta T_{II} = T_{h,o} - T_{c,o} \,. \tag{30}$$

The inlet temperature and outlet temperature of the hot fluid and the inlet temperature and outlet temperature of the cold fluid in the heat exchanger are expressed by $T_{h,i}$, $T_{h,o}$, $T_{c,i}$, $T_{c,o}$, respectively.

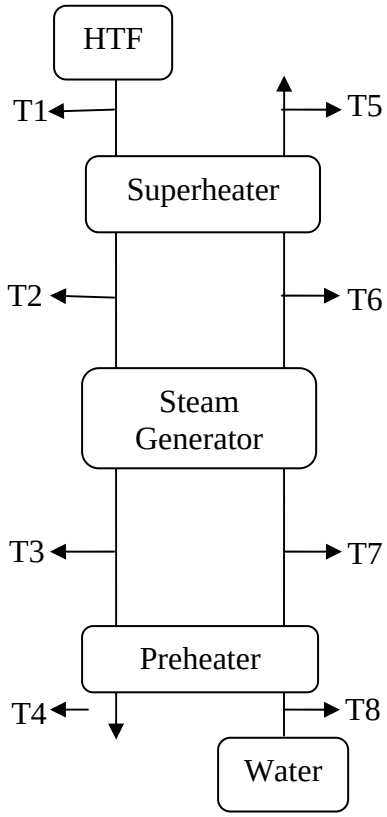

Figure 12: Temperature assignments for the steam train

The mass flow rate of the HTF and T1, the HTF temperature entering the steam train, shown in Figure 12, were known values. An optimization routine that solved the state points for the steam generator and superheater was also written to establish the mass flow rate of water across the steam generator. The water mass flow rate set the pressure for the turbine entrance and pressure drop on the working fluid side of the heat exchangers was neglected. Temperatures T6 and

T7 were assumed to be the saturation temperature set by the steam pressure. The optimization routine minimized the energy difference between values calculated for the energy balance and the effectiveness-NTU method. The UA values shown in Table 1 were used as the design UA values for both the oil-water and the salt-water heat exchangers.

Table 1: UA values for steam train

Heat Exchanger	UA kW/°C
Superheater	298
Steam Generator	2051
Reheater	653

Table 2 shows the design values for temperatures, pressures, and mass flow rates presented by Lippke [8] and the results from this study. Temperatures refer to the locations specified in Figure 12.

Table 2: Heat transfer design conditions for steam train heat exchangers

		P initial bar	P final bar	m oil kg/s	m water kg/s
Kearney		103.42	100	345.5	38.8
Results		100	100	345.5	39.2

	T1 °C	T2 °C	T3 °C	T4 °C	T5 °C	T6 °C	T7 °C	T8 °C
Kearney	390.56	377.22	317.78	297.78	371	313.89	313.89	234.83
Results	390.56	380.78	318.48	300.03	377.4	311.61	311.61	241.56

Once the mass flow rate of steam was determined, the design values for the reheater, shown in Table 3, were solved by simultaneously solving the two heat transfer equations. The flow rate for oil in the steam train was 87.2% of the total HTF flow rate and 12.8% went to the reheater during all power generating conditions.

Table 3: Reference conditions for reheater temperatures

	T1 °C	T2 °C	T3 °C	T4 °C	P initial bar	P final bar	m oil kg/s	m water kg/s
Kearney	390.56	297.78	208.67	371	18.58	17.099	50.9	33.04
Results	390.56	287.4	205.17	367.89	17.3	17.3	50.68	33.28

Oil-Salt and Salt-Oil Heat Exchangers

The design flow rate for salt during charging and discharging was determined by an energy balance that calculated enthalpy values for the temperature profile shown in Table 4. Ts and To are the temperatures for the salt and oil, respectively. The design charging flow rate for salt is equivalent to 2,350,800 kg/hr. The density of solar salt was calculated at 386°C to be 1844.5 m^3/kg, so the volumetric flow rate was found to be 1274.5 m^3/hr. The amount of salt needed for the Storage Oil-Water case will be equal to the number of hours of storage times the hourly volumetric flow rate. Storage Salt-Water, however, requires the number of hours of storage plus additional salt for operating the

plant. The amount of additional salt will depend on the cycle time through the power block.

Table 4: Design conditions for oil-salt heat exchangers

	Ts Hot °C	Ts Cold °C	To hot °C	To cold °C	flow rate kg/s
Charging	386.00	293.00	393.00	299.00	396.00
Discharging	386.00	293.00	379.00	287.00	396.00

	Q oil kJ/s	flow rate salt kg/s	LMTD °C	UA kW/°C	flow rate ratio Salt/Oil
Charging	91231.71	653.38	6.49	14063.43	1.65
Discharging	87986.27	630.14	6.49	13563.14	1.59

Less heat can be transferred back to the oil due the temperature constraints. An interesting consequence is that less salt is needed for discharging. The difference in salt results in an extended discharging period for Storage Oil-Water compared to Storage Salt-Water.

Salt-Water Heat Exchangers

The optimization code that was applied to the oil-water steam train was applied to the salt-water steam train, where nitrate salt thermal properties replaced oil thermal properties. Table 5 shows the design flow rate for steam is 36.23 kg/s, 3 kg/s less than the oil-water steam train. This decrease in flow rate

is reflected in the operating pressure which drops to 93.3 bar from 101 bar. Less power is expected to be generated from the salt steam train. Additionally, the turbine will experience more time in the saturation region due to the lower pressure.

Table 5: Design conditions for molten salt steam train

	T1 °C	T2 °C	T3 °C	T4 °C	T5 °C	T6 °C
Salt	386	375.74	314	298.47	372.83	305.8
Oil	390.56	380.78	318.48	300.03	377.4	311.61

	T7 °C	T8 °C	P initial bar	P final bar	m oil kg/s	m water kg/s
Salt	305.8	237.05	93.1	93.1	569.4	36.2
Oil	311.61	241.56	100	100	345.5	39.2

Replacing synthetic oil with molten salt in the steam train heat exchangers significantly affects the power block. A real plant with a molten salt steam train may be designed differently than assuming the same arrangement. Nexant Inc. [18] resolved this issue by modifying the design of the molten salt steam generation system and their work is shown in Figure 13. The molten salt used in the superheater and the reheater mix and together go to the steam generator. Salt temperatures were higher than 390 °C, which is greater than the upper limit of present HTF. Therefore their design values could not be extrapolated for this

study. In addition, their design cannot be readily compared to the SEGS VI design because the power block would require modification.

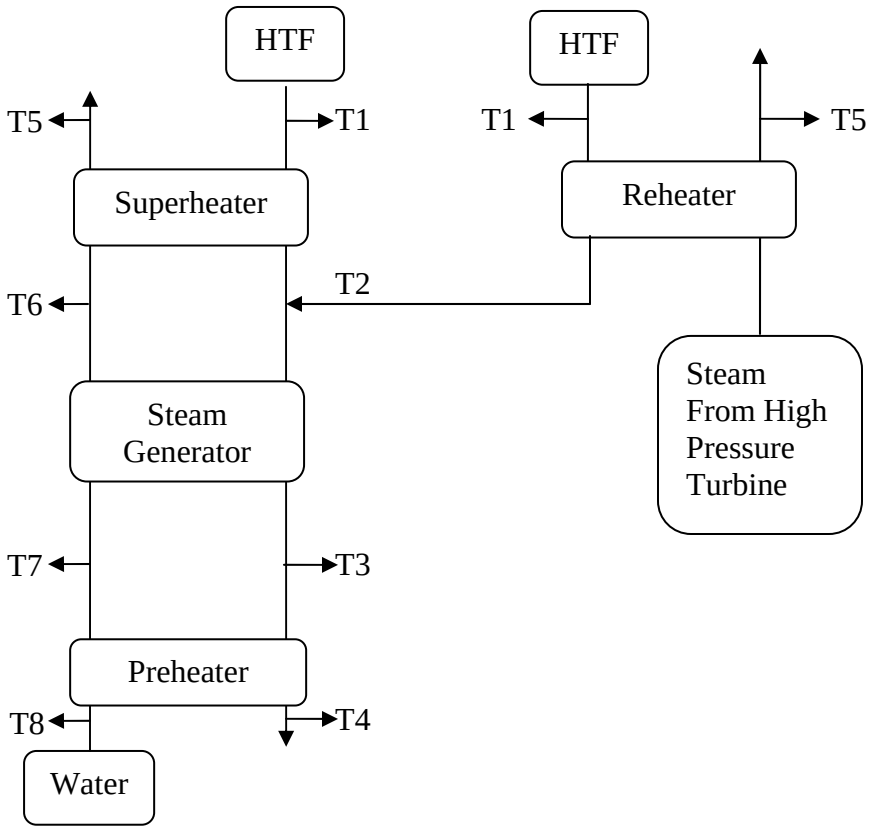

Figure 13: Representation of Nexant [17] molten salt steam train

Turbine

For all three power plant designs the turbine parameters were assumed to be identical. The only variables that would change were the input values of inlet temperature, pressure, water flow rate, and reheat inlet temperature. The salt

steam train is disadvantageous as a result because the turbine stages were built for a higher pressure.

The steam enthalpy at the high pressure turbine inlet was determined by the temperature and pressure solved in the superheater component. The enthalpy for the low pressure turbine inlet was determined by the same method for the reheater component. The inlet enthalpy for every other turbine stage was equal to the enthalpy exiting the prior turbine stage. The outlet enthalpy was calculated using the reference turbine stage efficiency and the isentropic relationship,

$$h_{out} = h_{in} - \varepsilon \cdot (h_{in} - h_{out\_isentropic}) \tag{31}$$

A perturbation was included by Patnode [10] where efficiency reduces as a function of steam mass flow rate.

$$\varepsilon_{decrease} = 0.191 - 0.409 \cdot (\frac{\dot{m}}{\dot{m}_{ref}}) + 0.218 \cdot (\frac{\dot{m}}{\dot{m}_{ref}})^2 \tag{32}$$

$$\varepsilon = \varepsilon_{ref} \cdot (1 - \varepsilon_{decrease}) \tag{33}$$

Adjusted design values for SEGS VI's power block components can be found in Lippke [8] and Patnode [10]. In solar literature, the mass flow rate and pressure drop through a turbine stage can be expressed in a relationship with their reference values. This is shown by

$$\frac{\dot{m}}{\dot{m}_{ref}} = \frac{P_1^2 - P_2^2}{P_{1ref}^2 - P_{2ref}^2}. \tag{34}$$

Accordingly, once the back pressure from the condenser is known, the pressure through the turbine can be back-calculated. However, Table 6 was tabulated by

equation 34 and shows the outlet pressure from the low pressure turbine does not affect the inlet pressure to the high pressure turbine.

Table 6: Correlation of turbine inlet pressure and water mass flow rate

T amb = 0 °C			
m water kg/s	P_{in} HP1 bar	Pin LP5 bar	Pin HP1/m water bar s / kg
5	12.853	0.037	2.5705
10	25.705	0.073	2.5705
15	38.558	0.108	2.5705
20	51.410	0.144	2.5705
25	64.263	0.180	2.5705
30	77.115	0.216	2.5705
35	89.968	0.252	2.5705
40	102.820	0.288	2.5705
T amb = 25 °C			
m water kg/s	P_{in} HP1 bar	Pin LP5 bar	Pin HP1/m water bar s / kg
5	12.853	0.060	2.5705
10	25.705	0.086	2.5705
15	38.558	0.118	2.5705
20	51.410	0.151	2.5705
25	64.263	0.186	2.5705
30	77.115	0.221	2.5705
35	89.968	0.256	2.5705
40	102.820	0.291	2.5705

Variance in the lowest pressure turbine stage due to ambient weather conditions does not affect the behavior of the high pressure turbine. Instead, the relationship used in this model was

$$P = 2.57 \cdot \dot{m}\,, \tag{35}$$

where $\dot{m}$ is the mass flow rate entering the high pressure turbine. This relationship was also useful in the optimization code for the mass flow rate of water in the steam train.

The power block model is a simplified version of the actual SEGS VI power cycle. Heat exchangers and turbine stages were described individually however models for the feedwater heaters, condensers, and cooling tower were not implemented in to the full cycle. The work of the cooling tower and condenser were assumed to cool the steam exiting the last stage of the turbine down to seven degrees above ambient temperature. This was considered acceptable for a dry cooling power plant. Further, the outlet pressure of the low pressure turbine was determined to be the saturation pressure at this temperature approximation.

Mixer and Power Plant Simplification

Two mixing units are utilized in both thermal storage designs. For the Storage Oil-Water one unit mixes oil from the solar field with oil heated from thermal storage. The second unit combines oil exiting the preheater, reheater, and the oil used to charge the thermal storage tanks. The Storage Salt-Water design utilizes a mixing unit with thermal storage discharge and another for mixing the salt after cycling through the power block. The total mass in the mixer is found by,

$$\dot{m}_{tot} = \sum_{1}^{i} \dot{m}_i \tag{36}$$

where *i* is the number of streams entering the mixer. The resultant enthalpy of the mixture is

$$h_{mix} = \frac{\sum_{1}^{i} \dot{m}_i \cdot h_i}{\dot{m}_{tot}}. \tag{37}$$

The cooling towers, condenser, feedwater heaters, and pumps were not included in this model. The second assumption made was the preheater inlet water temperature was a fixed the outlet water temperature. This value would be found by modeling the series of 5 closed feedwater heaters, a pump, and the open feedwater heater. Accurate parasitic calculations should be included in the next modeling generation. This will include the modeling the missing components and the power required to propagate the cycle.

Storage Tanks and Storage Controls Logic

The hot and cold storage tanks for Storage Oil-Water were identical with only the temperature of salt varying. The Storage Salt-Water case required a cold tank with an increased volume of one extra hour of salt. Each tank was assumed to be fully mixed thermally. The fluid volume in the tank had the capability to completely fill and discharge for every tank. The real limitations clarify that the salt cannot fully discharge nor does it completely fill the tank [13]. For a desired increase in thermal storage, the tank volume and area must increase.

The dimensions of the storage tank were meant to mimic the aspect ratio of the Andasol One storage tanks [4]. Those dimensions were a 39 meter diameter and a 19 meter tall tank. Above 11.7 meters the tank became conical, so the

height was approximated to be 11.7 meters. Power losses were reported 239 kW and 259 kW lost for the cold tank and hot tank respectively. Given an area of 3823 m^2, the heat loss terms can be expressed as 63 W/m^2 and 67.7 W/m^2. The aspect ratio of the storage tanks diameter to height was preserved for resizing the storage tanks to fit a 35 MWe plant. Table 7 displays the sizing requirements for the storage tanks for the amount of hours in storage. The amount of mass is the value calculated for the iteration interval of one second.

Table 7: Physical properties of thermal storage tanks

Salt Flow Rate m^3/hr	Discharge Time Hours	Volume m^3	Diameter m	Height m	Area m^2	Q Cold Tank MJ	Mass kg
1274.5	2	2549	22.045	6.68	1226.03	1138.62	1306
1274.5	4	5098	27.77	8.42	1945.51	2277.24	2612
1274.5	6	7647	31.79	9.63	2549.55	3415.87	3918
1274.5	8	10196	34.99	10.60	3088.66	4554.49	5224
1274.5	10	12745	37.7	11.42	3585.62	5693.11	6530

The energy balance for the mass of the tank was

$$M_{\tan k} = M_{\tan k}' + \dot{m}_{in} dt - \dot{m}_{out} dt \tag{38}$$

where $M_{\tan k}'$ is the mass of the tank from the previous iteration. Heat into the tank, Q_{in}, and out of the tank, Q_{out}, were solved by

$$Q = \dot{m} \cdot cp \cdot T \tag{39}$$

with T in absolute temperature in Kelvin. The heat in the tank was found by

$$Q_{\tan k} = Q_{in} - Q_{out} - Q_{loss} \tag{40}$$

A 100 °C difference in Nitrate salt only affects its specific heat by one percent. This error was considered negligible and the specific heat was treated as a constant.

The temperature in the storage tank was found by determining the temperature drop in the tank due to heat loss,

$$dT = \frac{Q_{loss}}{M_{\tan k} \cdot cp} \tag{41}$$

and tank temperature was thus calculated at the end of the time step

$$T_{\tan k} = T_{\tan k}' - dT \; . \tag{42}$$

Heat loss and the associated temperature drop for an isolated 6 hour tank of molten salt initially at 293 °C is shown in Figure 14. The heat loss term is based on area of the tank and not the volume of salt so the linear behavior is expected. Schulte-Fischedick [13] report the local solidification temperature for nitrate salt, 239 °C, is reached after 46 days for a half full tank with the capability of 7 hours of storage. Local solidification was reached in the tank in Figure 14 after 42 days, which is within a reasonable range of the published study.

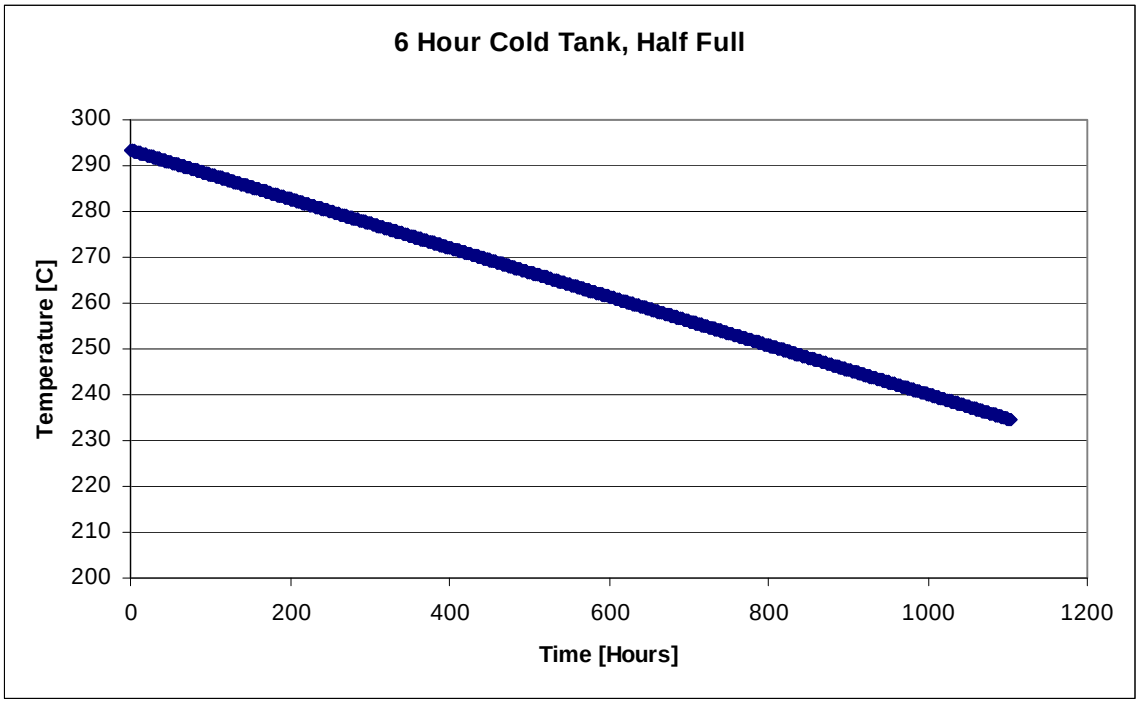

Figure 14: Temperature loss in 6 Hour Cold Tank, half full

When the tank is only 20% full, local solidification occurs after 17 days. A decreasing salt volume in one tank will yield more rapid temperature drop. A more detailed model of the tanks will examine the heating requirements needed for the hot tank and the cold tank because a minimum volume of salt must remain in both tanks. Another concern is how much temperature decrease is acceptable in the hot tank.

Other tank heat loss relations exist and could be explored. Discharging molten salt from the hot tank is known to cause a decrease in temperature for the remaining fluid in the hot tank to decrease. This is not only due to heat loss but also of thermal stratification in the tank. Though not as extreme as a thermocline

storage system, stratification within each tank could be modeled in the next generation of the code.

The basic thermal storage operating strategies for Storage Oil-Water and Storage Salt-Water are shown in Figure 15 and Figure 16. Advanced thermal storage controls will be valuable when parasitic calculations are analyzed. For example, the minimum amount of hot salt discharge necessary to produce net power could be determined.

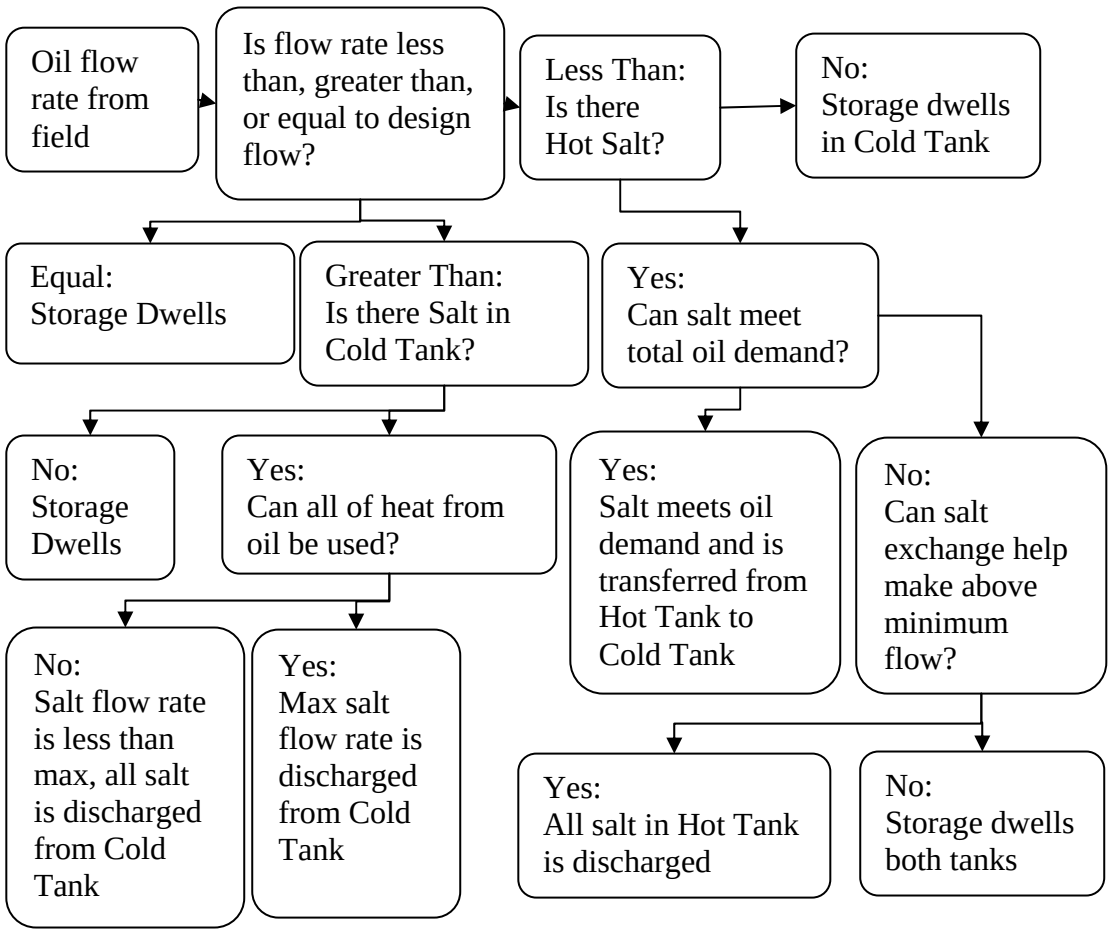

Figure 15: Storage Controls for Storage Oil-Water case

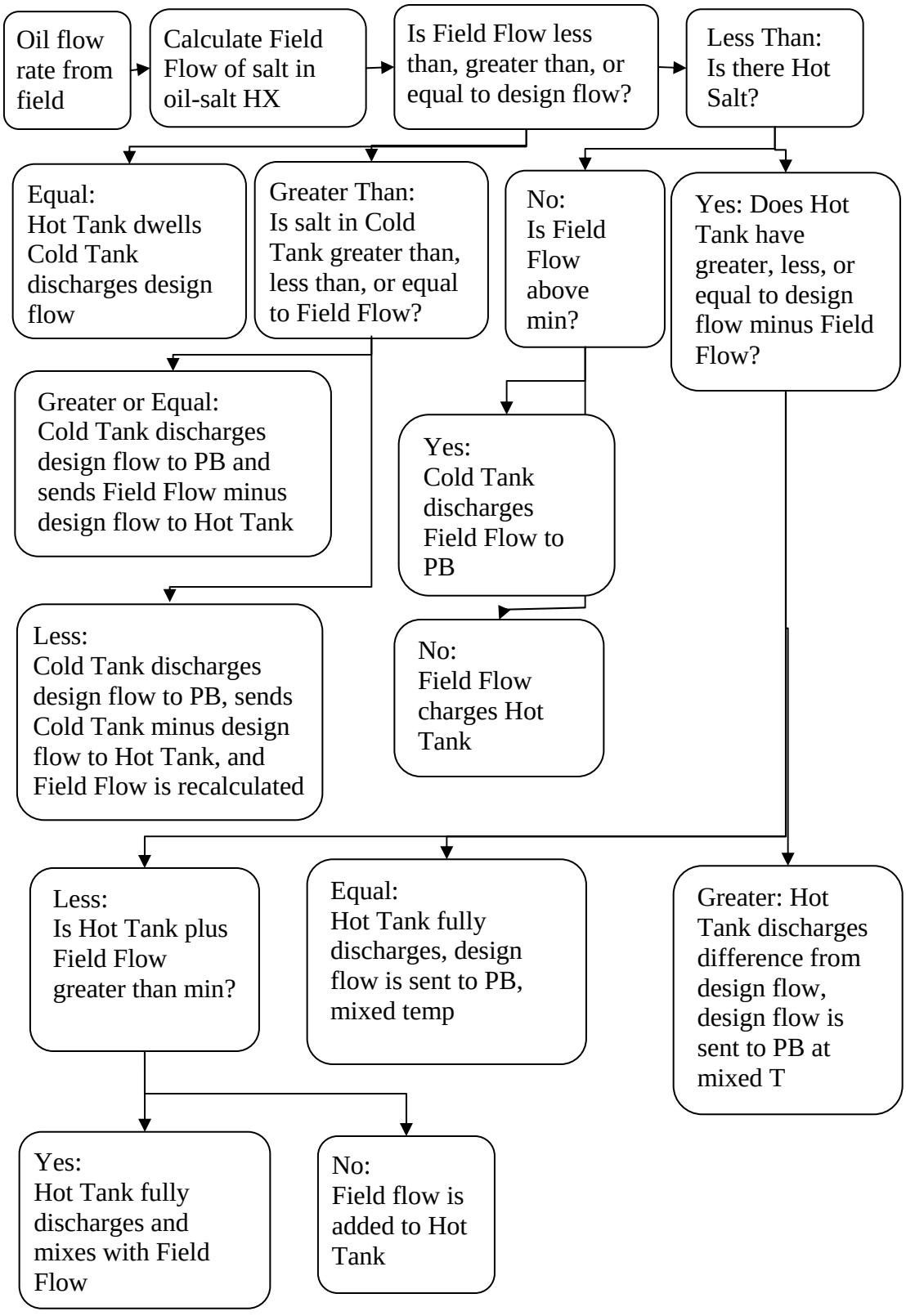

Figure 16: Storage controls for Salt-Water Storage

CHAPTER 4

RESULTS

No Storage

Three days were chosen to illustrate the behavior of the No Storage power plant under varying weather and climactic conditions. The summer day chosen was July 7th and it represents the ideal conditions for a solar parabolic trough power plant. The Southwestern deserts are known for afternoon stormy conditions in late summer. August 6th was chosen to represent a summer day with typical cloud cover in the early afternoon. This day is particularly important because of low solar radiation yet still a high demand for electricity, primarily due to air conditioning. Winter conditions in Las Vegas are sunny, but the low elevation of the sun increases reflection losses and will decrease the amount of energy that can be absorbed by a parabolic trough power plant because it is a single axis tracking technology.

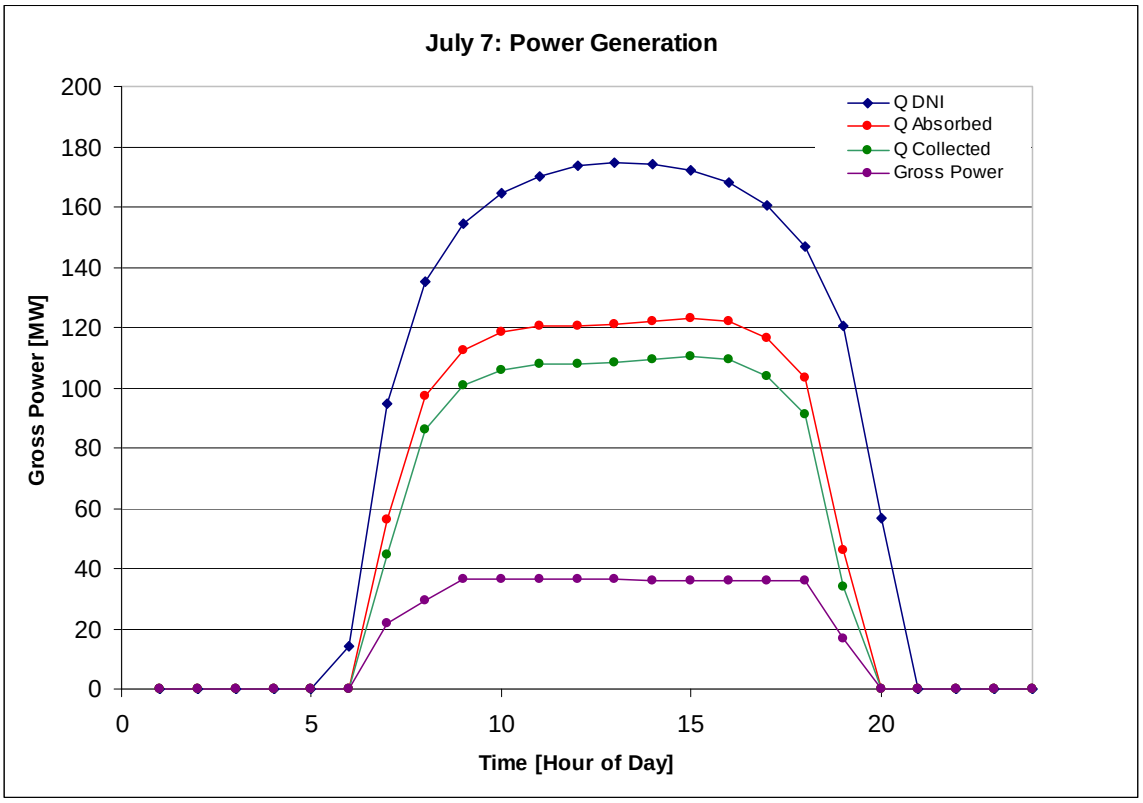

Figure 17: Hourly power totals for July 7, a typical sunny day

Figure 17 shows that energy generation on a clear summer day remains steady through out the day. Power generation is delayed in the morning and evening partially due to the troughs not tracking within ten degrees above the horizon. The difference between the energy absorbed and the energy collected is due to thermal losses in the solar field.

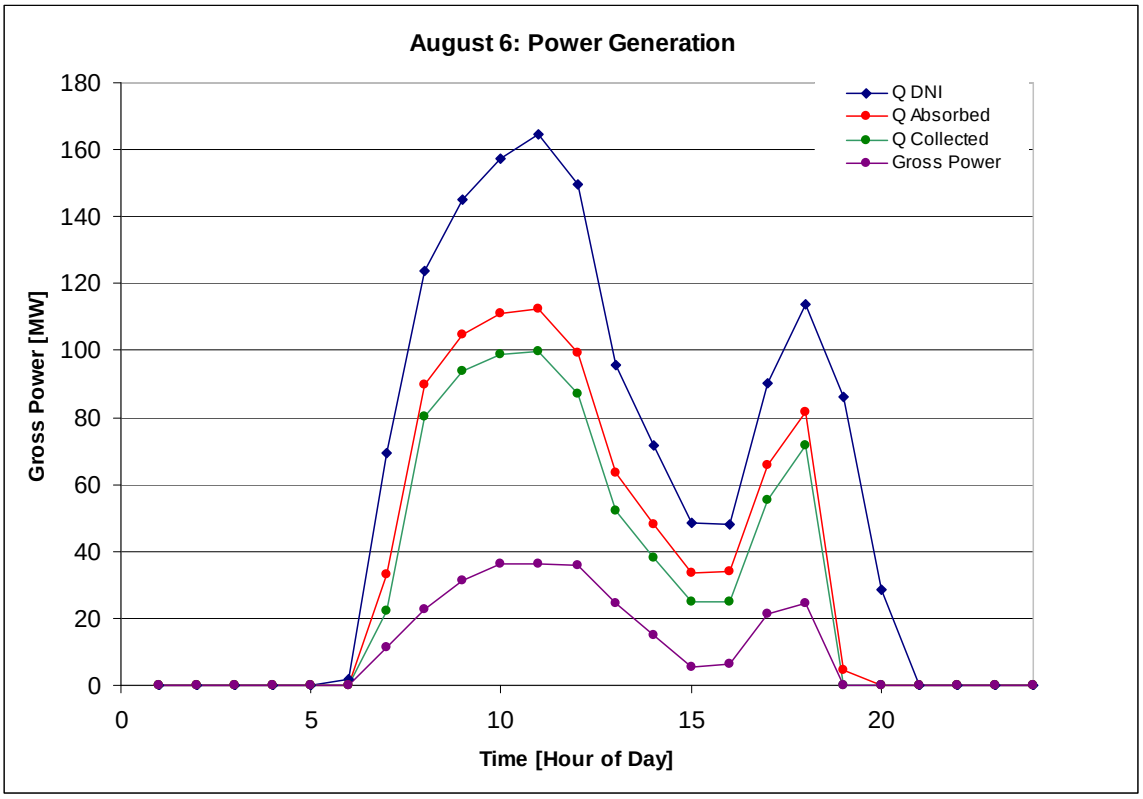

Figure 18: Hourly power totals for August 6, a day with afternoon clouds

The model demonstrates accurate reflection of the ambient weather conditions in Figure 18, when clouds arise at noon. Power generation is significantly reduced by low DNI in the early afternoon, yet the slope of gross power is not as steep as the slope of the solar field outputs.

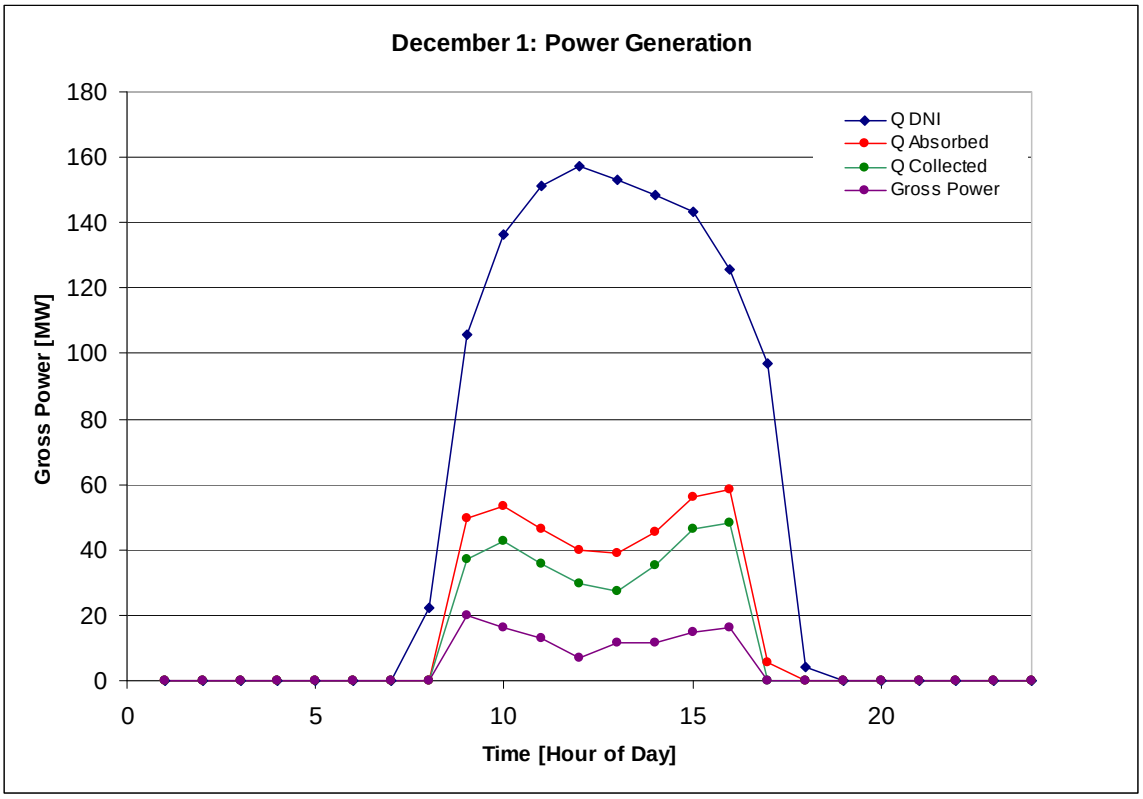

Figure 19: Hourly power totals for December 1st, a clear winter day.

Despite the high solar radiation, Figure 19 shows less energy is absorbed by the solar field in winter due to reflection losses due of the incidence angle.

Two acceptable methods of increasing annual energy generation for a given power block size are to increase the solar multiple or to add thermal storage. An actual plant is not likely to incorporate thermal storage after it is built but it is possible for a plant to increase the size of its solar field.

An increase in solar multiple is not beneficial for the entire year. Figure 20 illustrates that all solar multiple values reach maximum power generation on July

7th. Potential thermal energy is wasted during the summer months even for a solar multiple of one. However, the revenue lost by wasting potential power must be compared to the cost of implementing thermal storage. A solar multiple of one will not waste enough potential power to justify thermal storage. The solar multiple has to increase for thermal storage to be a significant contributing factor to the plant.

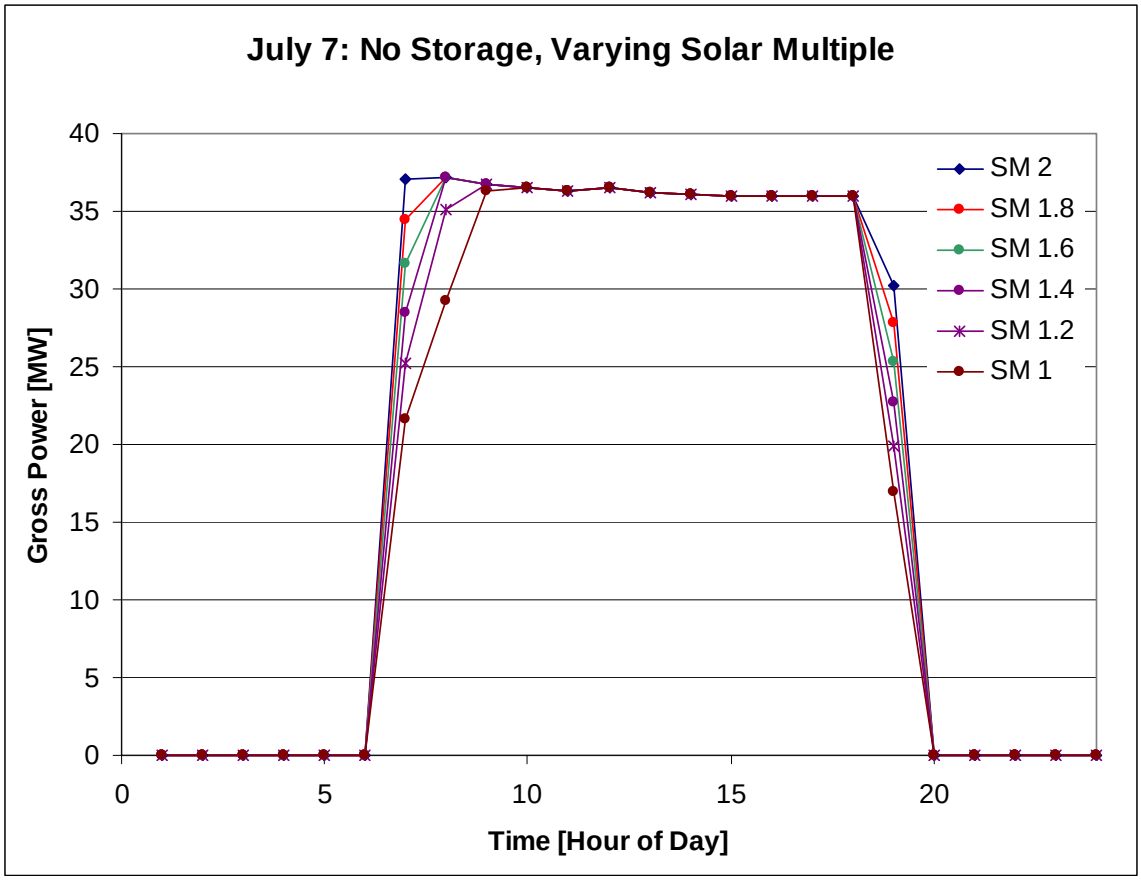

Figure 20: Gross power generation for July 7 with several solar field sizes

Additionally, the simulation confirmed that at SM 1.6 the mass flow rate exceeded double the design flow rate. This signifies more oil-salt heat exchanger area is needed for solar multiples greater than 1.6.

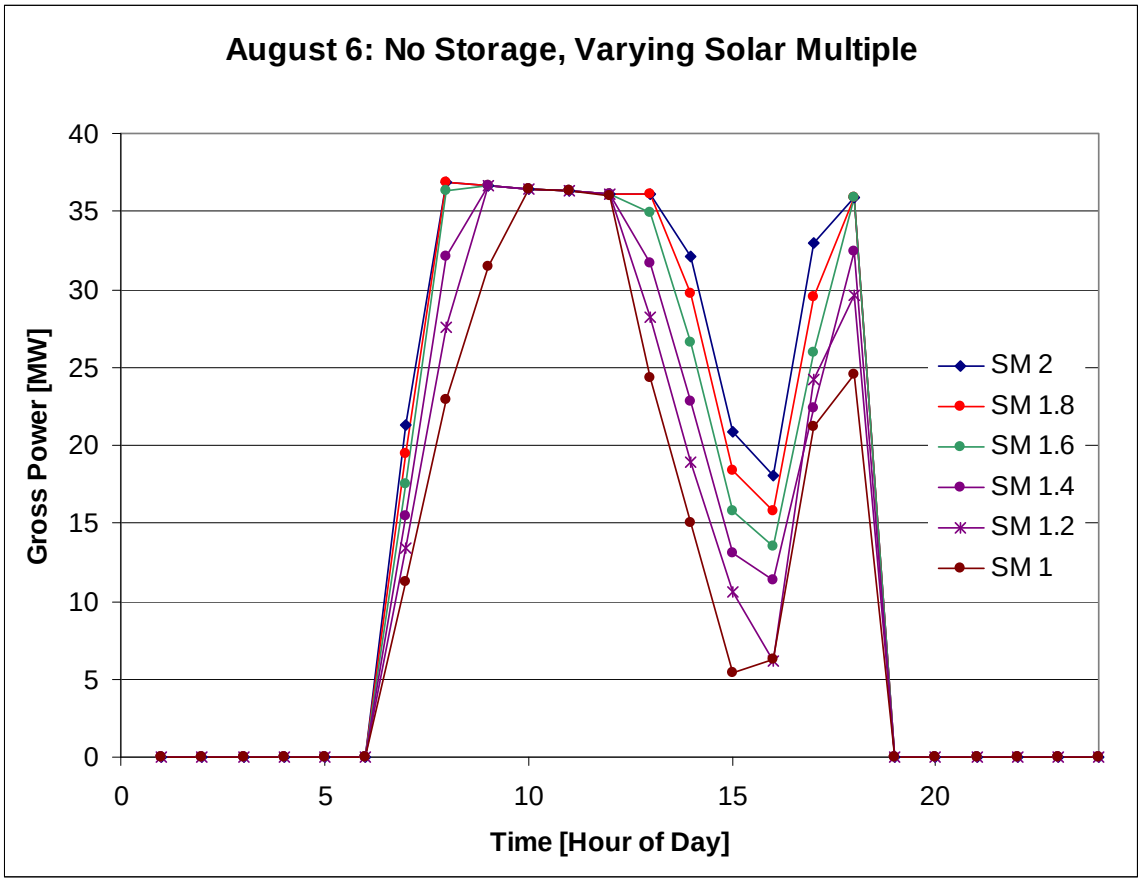

Figure 21: Gross power generation for August 6 with several solar field sizes

The solar field size becomes more relevant for a summer day that becomes cloudy, such as August 6th, presented in Figure 21. The solar multiples greater than one waste more potential thermal energy in the morning but aid in maintaining higher power generation during the cloudy period.

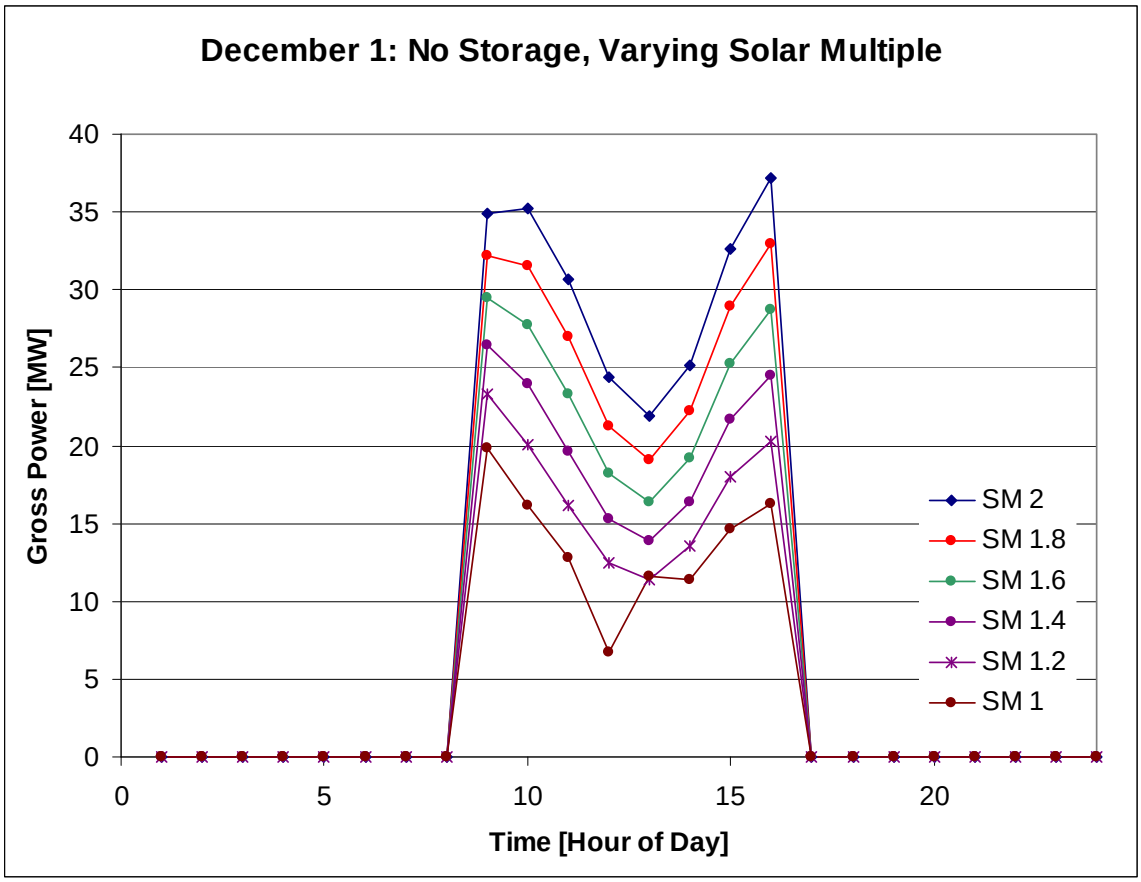

Figure 22: Gross power generation for Dec 1 with several solar field sizes

The overall trend in Figure 22 shows significant improvement in power generation by augmenting the solar field size. The data point at 1 PM for the SM1 curve in is inconsistent with the other solar field sizes. The discrepancy is due to a sensitivity issue in the steam generation optimization routine that only occurs when the oil mass flow rate is in the range of 40-80 kg/s. A secondary convergence criterion should be explored for the optimization routine.

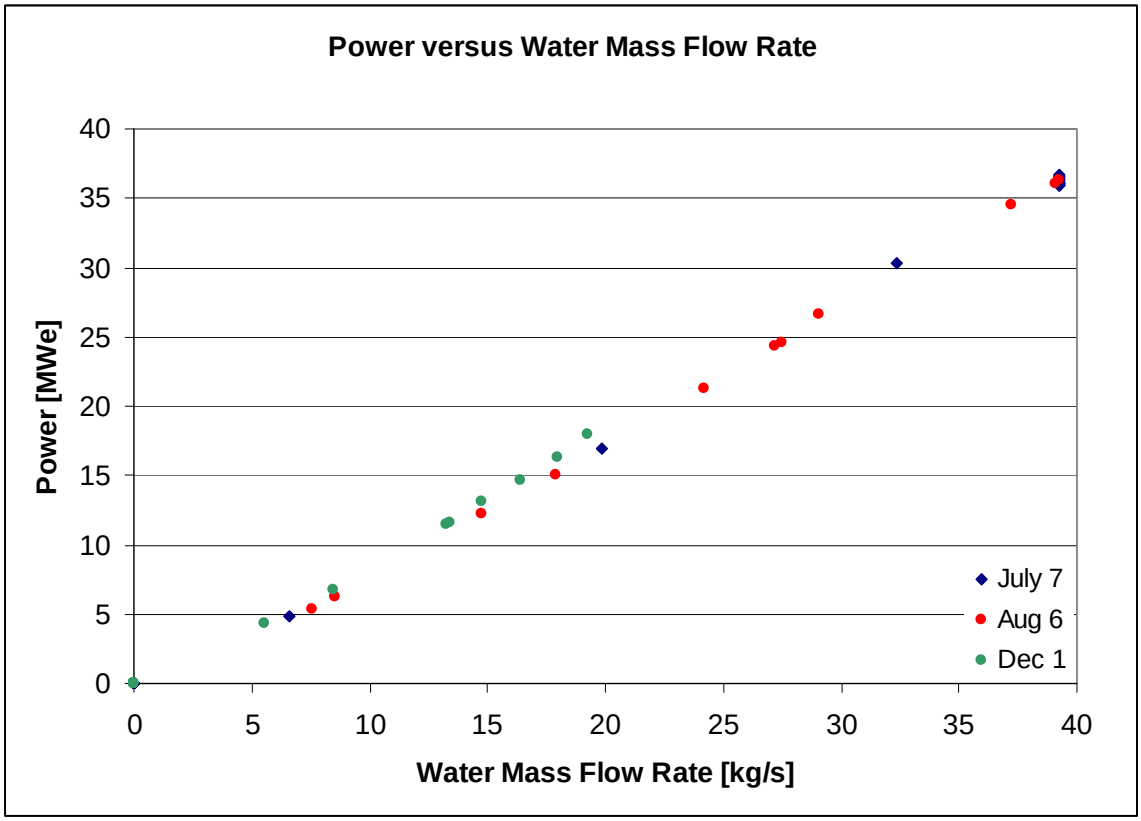

Figure 23: Power versus water mass flow rate for the No Storage case

According to Figure 23, for SM 1 without storage, power generation appears to be linearly related to water mass flow rate. A linear regression could be developed to simplify the calculations for the power block. However, the heat exchanger equations would still have to be calculated for the balance of the plant. Or, the regression would have to include the inlet temperature of the hot fluid in steam generation as an input and the hot fluid outlet temperature as an output.

The optimization code written to determine the mass flow rate of the water is dependent on the inlet heat transfer fluid temperature. A decrease in the quality of the heat transfer fluid temperature will decrease the water flow rate. Therefore the temperature exiting thermal storage will contribute to the amount power generated.

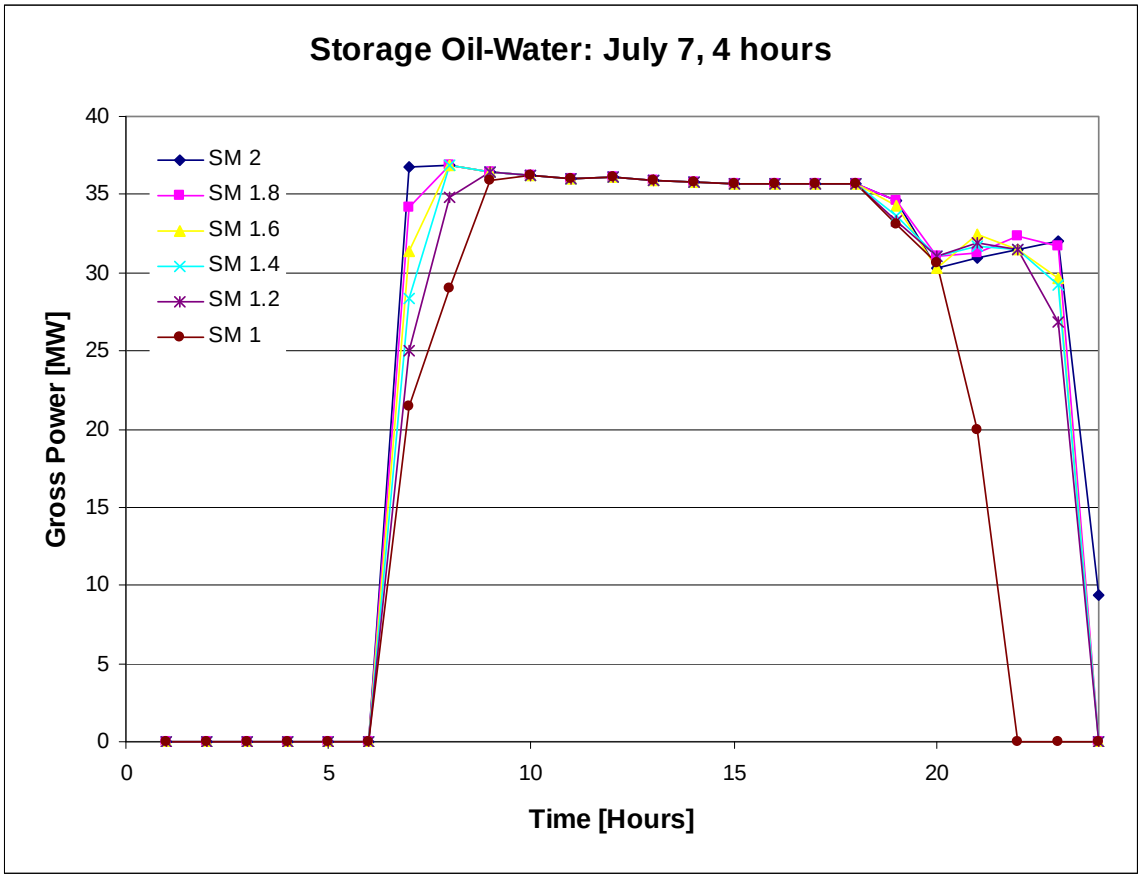

Figure 24: July 7th with four hours of thermal storage, varying solar multiple

The power generated after 6 PM in Figure 24 represents the expected behavior of the power generated from thermal storage. The decrease in power is due to the HTF temperature drop from the increased number of heat exchangers.

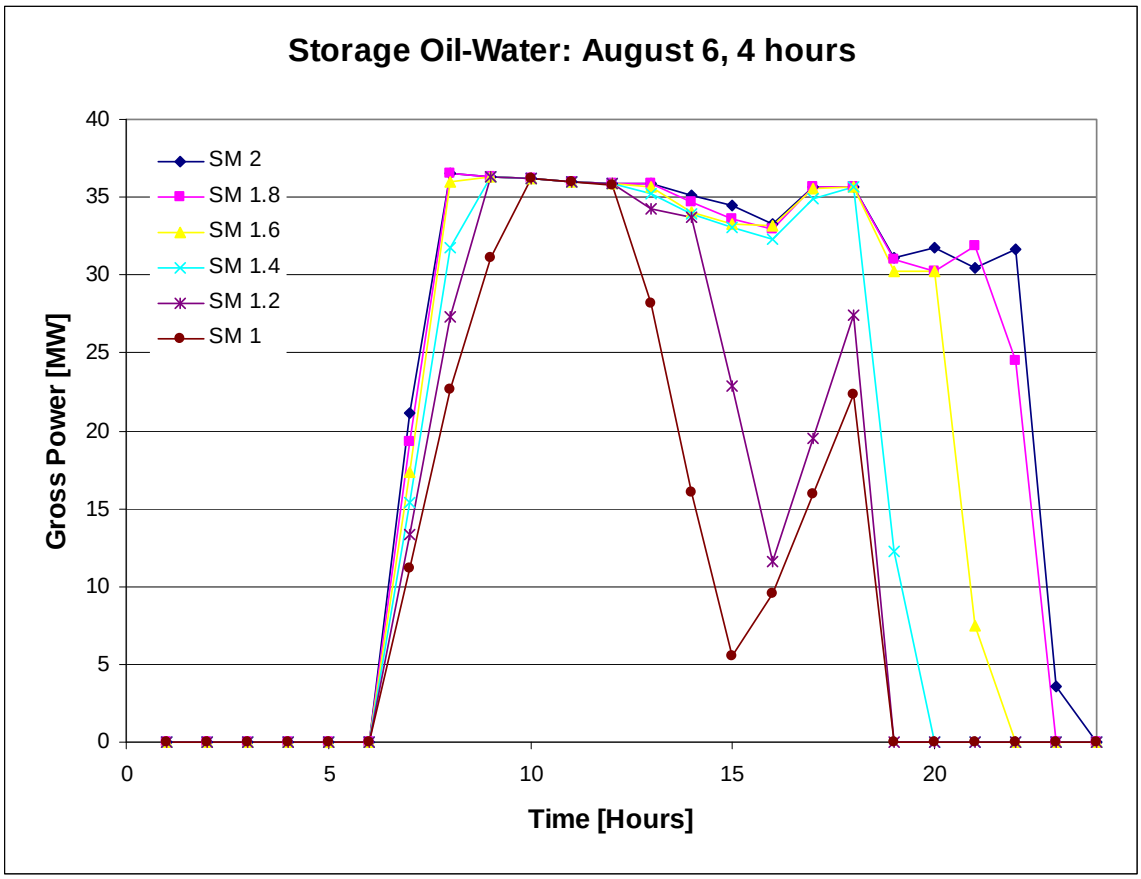

Figure 25: Aug 6th with four hours of storage, varying solar multiple

Four hours of thermal storage and SM 1.4 or greater will provide enough thermal energy in Figure 25 to overcome the cloudy weather for August 6th. At 1 PM thermal storage is discharged and the solar multiples of 1 and 1.2 did not have enough thermal storage to generate power at full capacity during the transient period. The increase in power generation at 5 PM is due to DNI returning to high values. The larger the solar multiple the longer into the evening

storage can provide power. Both SM 1.8 and SM 2 are able to full charge the four hour tanks.

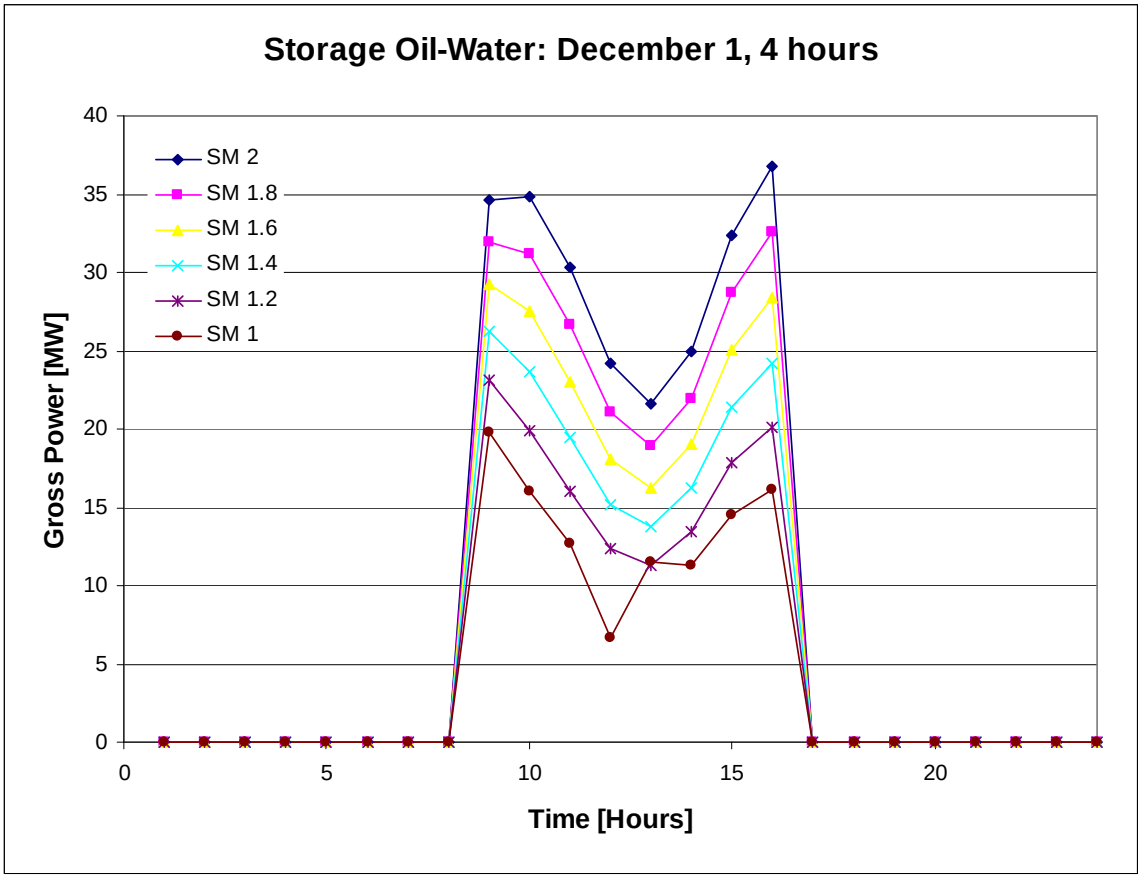

Figure 26: Dec 1st with four hours of storage, varying solar multiple

Despite doubling the solar field size, Figure 26 illustrates that some winter days will not be able to utilize thermal storage. Too many consecutive days with similar conditions will require the use of auxiliary heating for the storage tanks.

There are clear differences between power generated by No Storage and Storage Oil-Water. While the increase in solar multiple aids the No Storage case, the value of an increase is more evident when thermal storage is implemented. The balance between the amount of storage and the size of the solar field is critical for cost analysis and power generation. The most cost effective solution will also depend on the location.

As the solar multiple and amount of storage increases the ability to produce power for longer hours continues to rise. The longest amount of thermal storage explored was 10 hours and Figure 27 demonstrates the results for July 7th. At SM 1.6 and above 24 hour power generation is achievable.

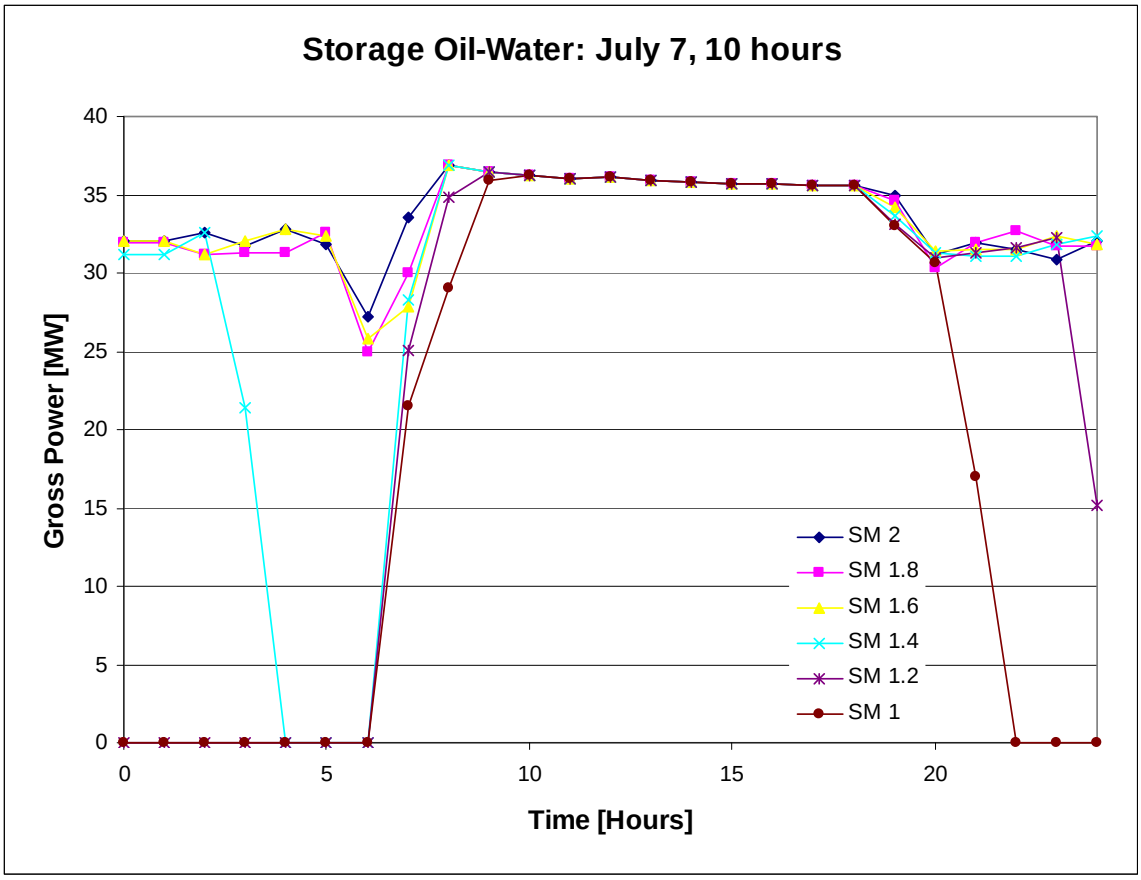

Figure 27: July 6th with ten hours of storage, varying solar multiple

This is realistic because SM 1 can collect 120% of the design thermal energy from the solar field when DNI reaches 1000 W/m². At SM 1.6 the thermal energy from the solar field will double design conditions, so for every hour of high solar insolation an hour of thermal storage can also be harvested. Power generation without thermal storage ceases at 8 PM. Thermal storage begins is fully utilized from 8 PM until 6 AM, a total of 10 hours. Due to some thermal storage utilized at 7 PM, the amount of thermal storage at 6 AM is less than full capacity. The 10 hours of thermal storage was found to be the minimum amount of storage to provide 24 hour electricity production.

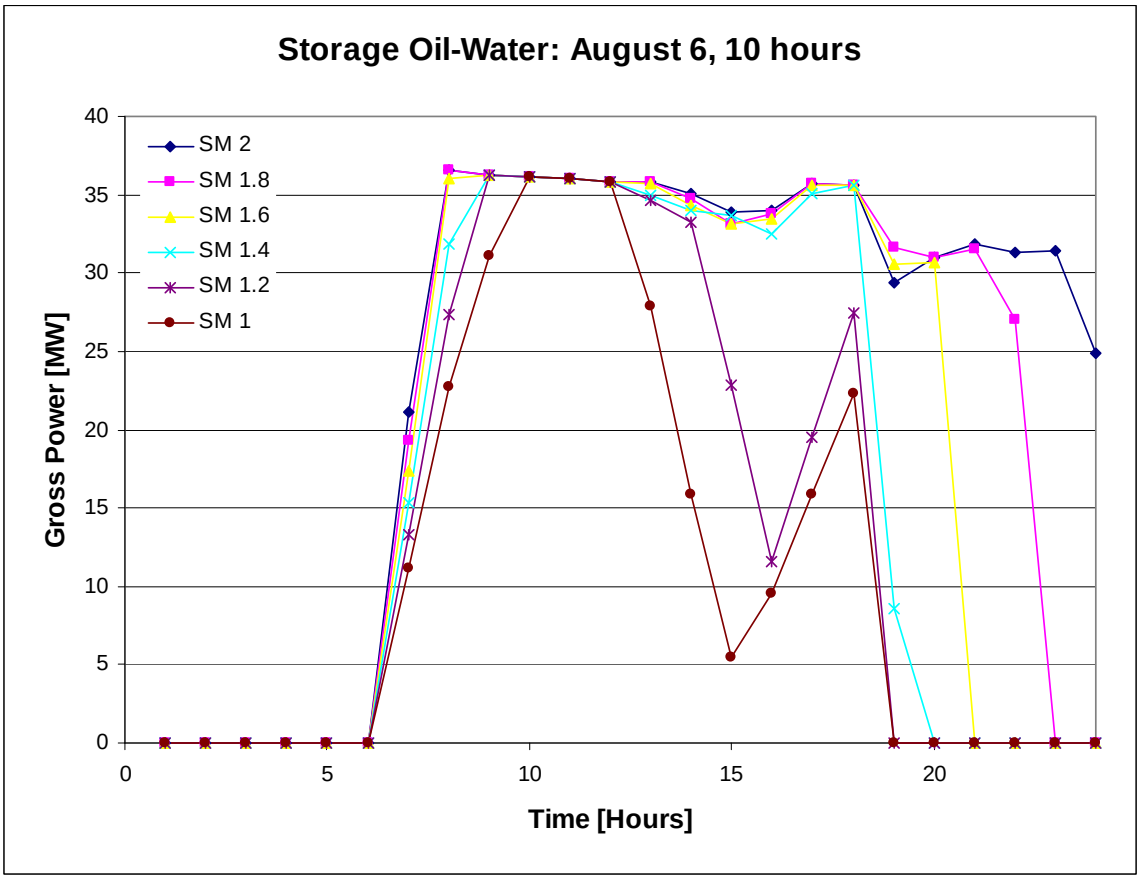

Figure 28: Aug 6th with ten hours of storage, varying solar multiple

The results for ten hours of thermal storage during a cloudy summer day, depicted in Figure 28, are similar to those of four hours of thermal storage. However, the total energy generation for the day is highly dependent on the solar field size.

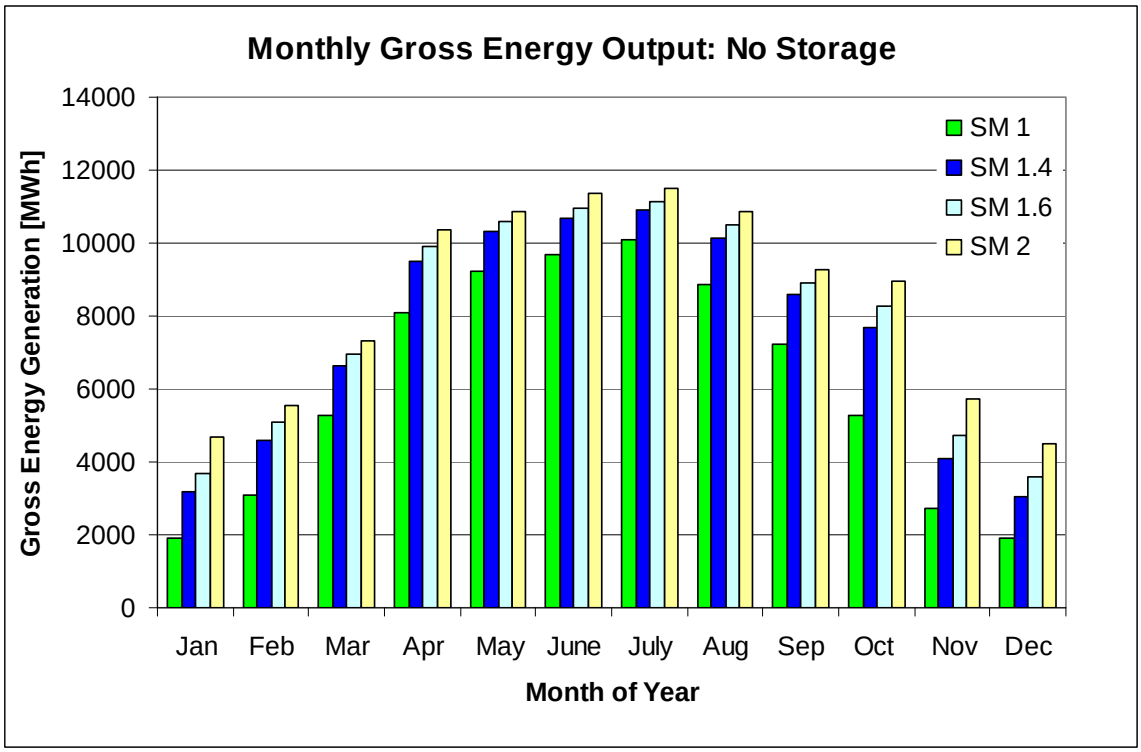

Figure 29: Monthly gross energy output for the No Storage Case

The trends of gross energy generation by month are shown in Figure 29. An increase in solar field area improves generation all year but is most important for a plant without storage during the non-summer months.

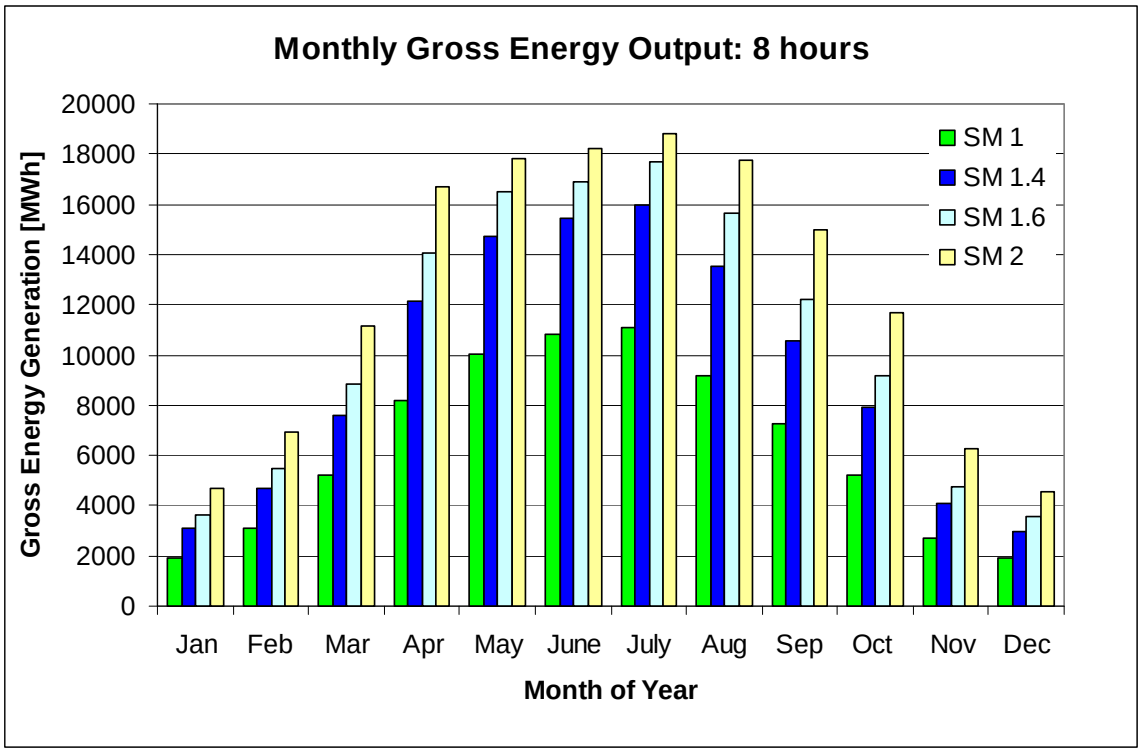

Figure 30: Monthly gross energy output for Storage Oil-Water with 8 hour tank.

The appreciable amount of energy that can be generated when storage is incorporated into the plant is evident in Figure 30. There is an increase of 1,000 MWh even for the SM 1 case during the summer months. For the SM 2 case, the increase is 7,000 MWh above the No Storage design.

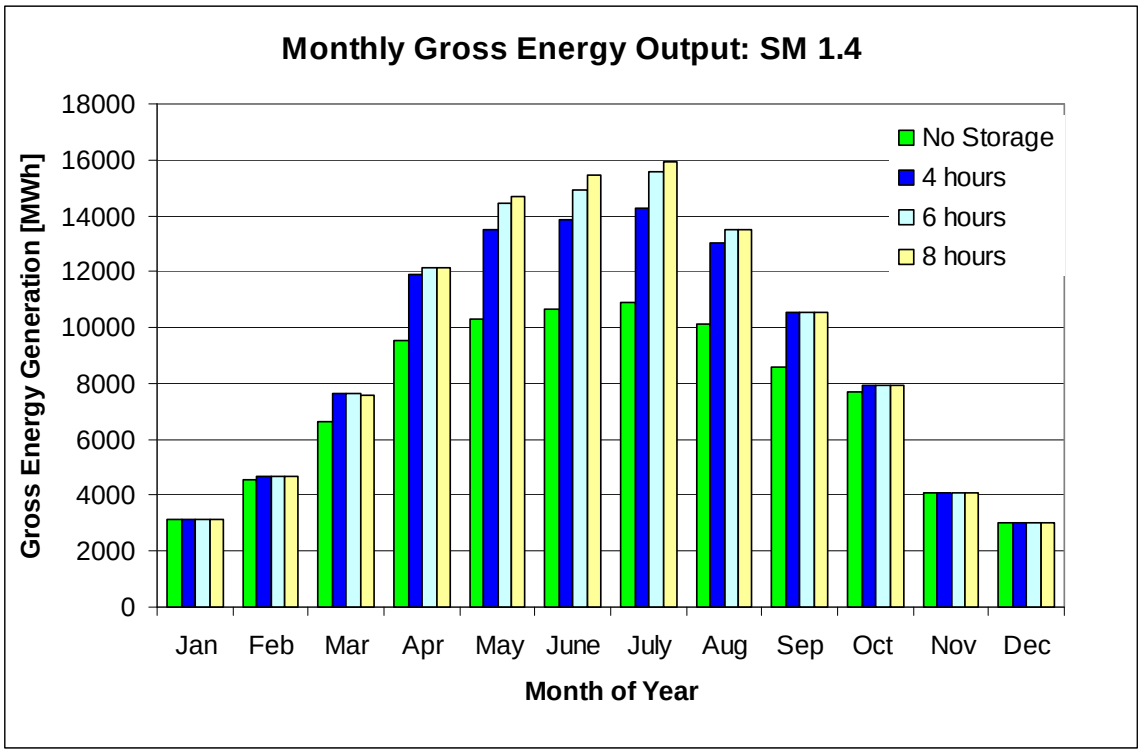

Figure 31: Monthly gross energy output for solar multiple of 1.4

Winter conditions clearly level the benefit of thermal storage, as seen in Figure 31. For a 1.4 solar multiple the differences in energy production from varied storage tanks size are only appreciable from May to August.

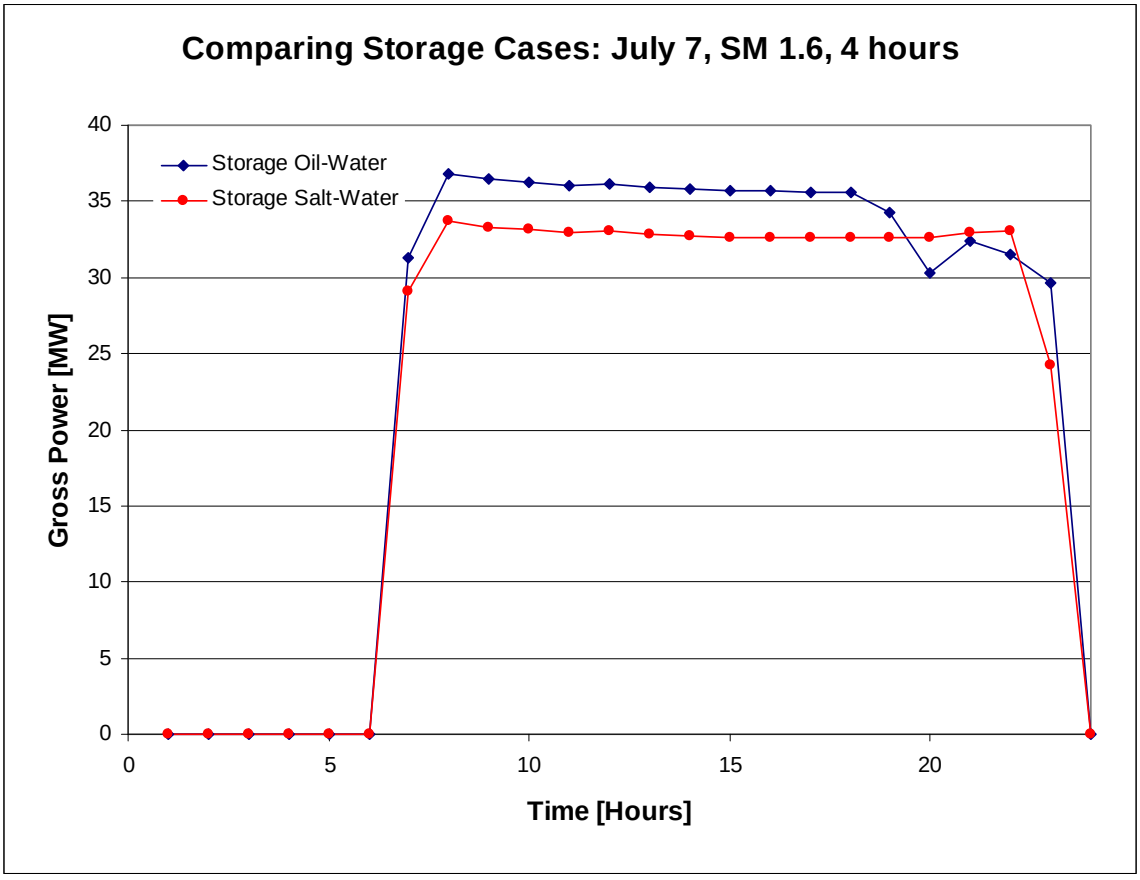

Figure 32: Storage designs for July 7, SM 1.6 and 4 hours of storage

The differences between the two thermal storage designs, shown by Figure 32, are very evident. The lower design flow rate for steam in the Storage Salt-Water case results in less power generation during normal operating hours. Also, the Storage Salt-Water case generates more power when the thermal storage provides the only heat source and the amount of power does not

decrease during discharging because the number of heat exchangers remains constant. However, this increase in power production from storage discharging is less than the power not produced during normal operating hours.

Additionally, the Storage Oil-Water design produces more power at the end of the day for two reasons. Less salt is needed for thermal discharging, which will extend hours of operation. However the more dominant cause is the amount of heat loss in the oil-salt heat exchangers. The three percent heat loss becomes a much larger amount when all HTF from the solar field transfers thermal energy into the molten salt.

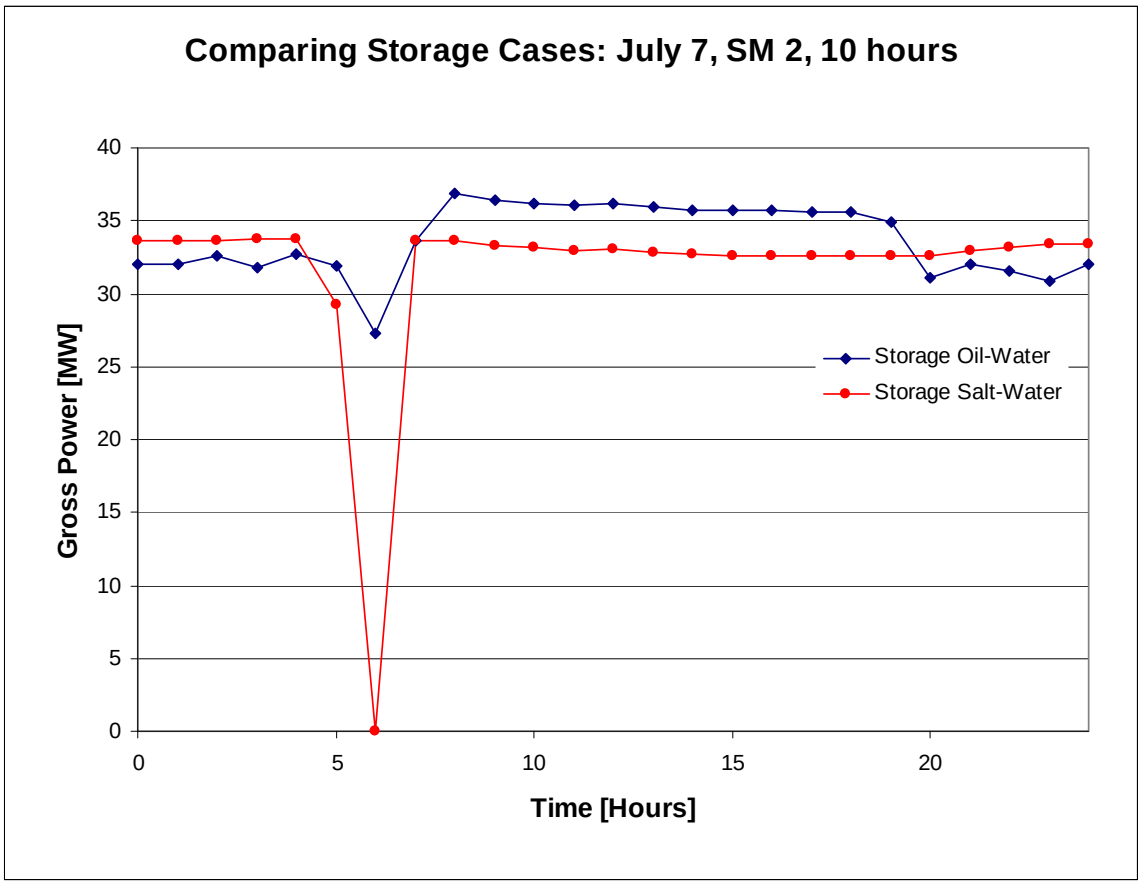

Figure 33: Storage designs for July 7, SM 2 and 10 hours of storage

The trend of longer power generation by Storage Oil-Water is more obvious in Figure 33, where the solar multiple increased to 2 and the storage tanks contain 10 hours of thermal storage. While Storage Oil-Water can provide 24 hours of power, Storage Salt-Water cannot. Increasing the solar multiple and the number of hours of storage will not favor Storage Salt-Water for this operating strategy.

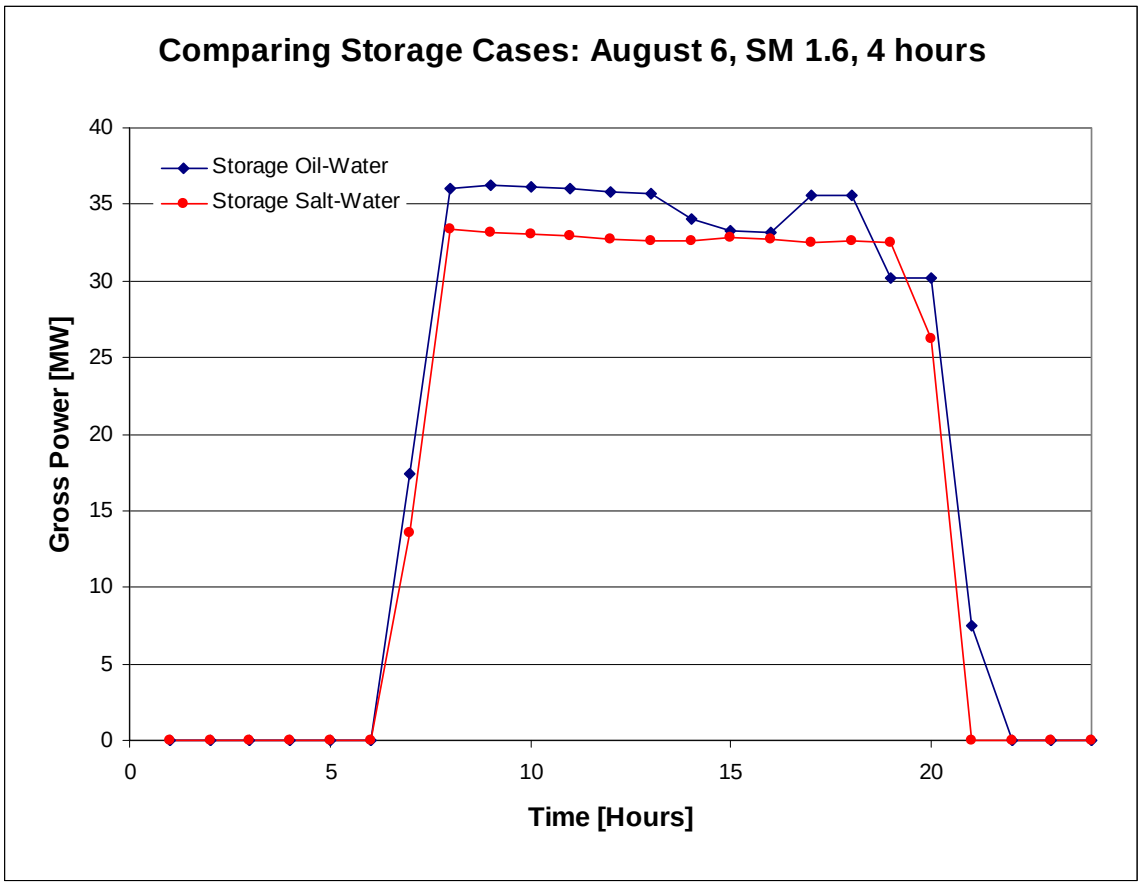

Figure 34: Storage designs for August 6, SM 1.6 and 4 hours of storage

Storage designs are compared for August 6th in Figure 34 and the power plants have enough thermal energy smooth over the transient afternoon weather conditions. At 1 PM thermal storage is discharged and Storage Oil-Water displays a decrease in power generation. However, because of a moderate level of DNI thermal storage is not needed to discharge at full capacity. During the afternoon transient hours, power production from Storage Oil-Water does not decrease below Storage Salt-Water power production levels.

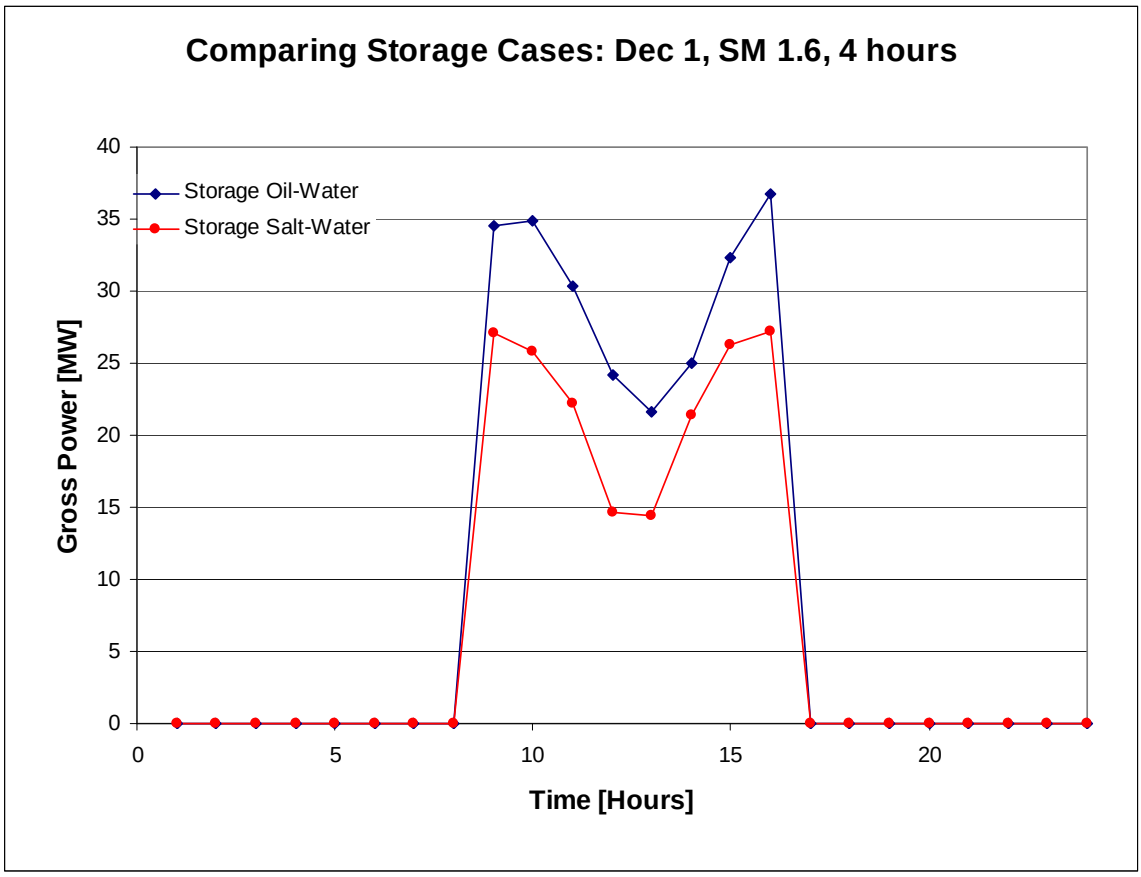

Figure 35: Storage designs for Dec 1, SM 1.6 and 4 hours of storage

The two curves in Figure 35 display the same trend for the winter conditions. Storage Salt-Water generates less power than Storage Oil-Water during off-design conditions. However, the molten salt is continuously cycled in Storage Salt-Water. This reduces the concern for solidification of the molten salt and will also reduce the amount of auxiliary heating needed, especially for low solar multiples.

The annual energy totals for the solar field and gross power generation are presented for the No Storage case in Table 8. An increase in solar multiple is followed by an increase in gross energy production, however the increase is non-linear.

Table 8: Annual energy totals for No Storage

No Storage	Incident	Absorbed	Collected	Gross Energy Production	
SM	MWh_{th}	MWh_{th}	MWh_{th}	MWh_e	(factor of SM1)
1	471721	256398	215960	81044	1.00
1.2	566065	307678	258510	90572	1.12
1.4	660409	358958	301038	97046	1.20
1.6	754753	410237	343574	101904	1.26
1.8	849097	461517	386079	105649	1.30
2	943441	512797	428614	108586	1.34

Table 9 shows the annual energy generation for each storage case examined divided by the annually energy of the No Storage case at solar multiple of one. This normalization neutralizes most operating assumptions and allows all annual energy totals to be compared to the relative performance of the bases case. When a plant incorporates thermal storage the rate of gross annual energy production is accelerated. Storage sizes greater than 4 hours are not useful for Storage Oil-Water at SM lower than 1.4 and for Storage Salt-Water at SM lower than 1.6. Tank heat loss even neutralizes the benefits of additional power production in some of these cases.

The same amount of energy is produced for Storage Oil-Water cases of SM 1.8 with 4 hours of storage and SM 1.6 with 6 hours of storage. Net power produced and an economic analysis of the cases would determine which condition will provide a better solution.

Accurate parasitic calculations will require several calculations not performed in the No Storage plant. The Storage Oil-Water design will need additional HTF pumping, salt pumping power between tanks, and auxiliary heating requirements. The storage Salt-Water design will require the pumping power for molten salt through the steam train and reheater, and auxiliary heating.

According to Table 9, Storage Salt-Water never produces the power that can be obtained from Storage Oil-Water. However, there are alternative operating strategies that highlight the advantages of Storage Salt-Water such as shifting power generation [19].

Table 9: Normalized annual energy generation

Storage Oil-Water

SM	No Store	2 h	4 h	6 h	8 h	10 h
1	1.00	1.04	1.04	1.05	1.04	1.04
1.2	1.12	1.22	1.27	1.28	1.27	1.27
1.4	1.20	1.33	1.43	1.49	1.50	1.50
1.6	1.26	1.42	1.55	1.64	1.70	1.73
1.8	1.30	1.49	1.64	1.75	1.85	1.91
2	1.34	1.54	1.71	1.85	1.96	2.05

Storage Salt-Water

SM	No Store	2 h	4 h	6 h	8 h	10 h
1	1.00	0.96	0.96	0.96	0.96	0.96
1.2	1.12	1.13	1.17	1.17	1.17	1.17
1.4	1.20	1.24	1.32	1.37	1.38	1.38
1.6	1.26	1.32	1.43	1.52	1.57	1.59
1.8	1.30	1.38	1.52	1.63	1.71	1.76
2	1.34	1.43	1.58	1.71	1.82	1.90

CHAPTER 5

CONCLUSIONS AND RECOMMENDATIONS

Matlab™ code was successfully written to simulate the gross power output for three solar parabolic trough power plant designs: No Storage, Storage Oil-Water, and Storage Salt-Water. The primary design parameters were extrapolated from SEGS VI, when applicable. The model behaves as expected to weather and seasonal changes. It deviates from SEGS VI's power output due to simplifications and differing operating strategies. The analysis of the competing thermal storage designs is valid as all three plant designs are compared on equal footing.

Several performance distinctions were identified between the two tank indirect thermal storage systems. Storage Oil-Water displayed a lower power output when thermal storage was the primary heat source. However, Storage Salt-Water did not produce as much power during normal operating conditions. This was due to a lower design temperature of salt at the power block heat exchangers entrance and also because nitrate salt has a lower heat capacity than synthetic oil. For the basic operating strategy examined, to maximize the amount of time operating at full-capacity, Storage Oil-Water showed better annual gross energy generation for all solar multiples and storage tank sizes.

A significant cost increase to Storage Salt-Water is the size of the oil-salt heat exchanger. Additionally, this increase in size led to greater heat loss when transferring thermal energy from oil to salt. However, the assumption that both

heat transfer fluids maintained identical UA values for the steam generation heat exchangers implies the Storage Salt-Water heat exchanger area will decrease. This will reduce the cost of the Storage Salt-Water unit. Auxiliary heating equipment will be necessary for both storage designs; however their presence in the Storage Salt-Water case is only a safety precaution because the salt is cycled daily.

The size of the storage tanks and the quantity of molten salt were identified. It was also determined that the volume of salt needed in Storage Salt-Water will increase to include the amount needed for the power block loop. Further analysis can also include component cost analysis, such as size of solar field and hours of thermal storage, that will help determine the most cost-effective plant for a desired annual energy generation total.

Parasitic calculations can be performed in the future to calculate the net annual power and to provide clear annual solar-to-electric efficiency values. Several parasitic relationships need to be identified including salt pumping requirements for both storage designs and auxiliary heating requirements. Pumping power will increase with the molten salt steam train due to a higher flow rate and a higher viscosity.

The optimization scheme used to solve the mass flow rate of the cooling fluid in the heat exchanger problems could use improvement, as evidence in the variability at low mass flow rates. Secondary convergence criteria could be explored. The alternate design for molten salt steam generation performed by

Nexant [18] would lead to a new power block optimization. This may improve the power generating capabilities of the Storage Salt-Water design.

Further operating strategies could modify storage controls to shift power generation to match peak demand hours. This would be desired by utility companies and they are likely to pay more for power produced during peak load demand. Shifting power generation may favor Storage Salt-Water because thermal storage will be utilized as the primary heat source for a greater amount of time.

APPENDIX A

MATLAB CODE

```
%Storage Salt-Water: SM 1, 4 hours storage
% JK 2009


    %Inputs

        Data=xlsread('Las_Vegas_TMY3.xls');
        Day=Data(:,1);
        Hour=Data(:,2);
        DNI=Data(:,3);
        Tamb=Data(:,4);
        WindSpeed=Data(:,5);

    %Location Parameters

        Long_L=115.08;              %Local Longtitude
        Long_St=120;                %Standard Longitude, GMT -8
        Lat=36.06;                  %Local Latitude
        phi=Lat*pi/180;             %Latitude in radians
        beta=0;                     %Slope from horizontal
       gamma=0; gamma_s=1;          %Surface azimuth angle... sine(0)=0


    %Solar Field Parameters
    %Units are m and m^2

        L_SCA_loop=753.6;           %Length of Solar Collector Assembly
         L_SCA=50;                  %Length of single collector
        L_spacing=15;               %Spacing between troughs
        Num_SCA=50*1;               %Number of SCAs
        W_SCA=4.83;                 %Width of Luz2 SCA
        SolarArea=L_SCA_loop*W_SCA*Num_SCA; %Solar Area
        Loops=Num_SCA/2;            %Loops treat hot and cold row
        FocalLength = 5;            %Focal Length of Trough
        T_f_o = 390.56;
        h_field_out=1000*(-18.34+1.498*T_f_o+0.001377*T_f_o^2);  %[J/kg]
        mdotField_ref = 396;

    %Heat Collection Element Parameters
```

```
    etaField=0.994*0.98*0.935*0.95;  %Eta Field = TrkTwstErr * GeoAcc *…
                                                  MirRef * MirCln
    etaHCE=0.98*0.99*0.963*0.95*0.96;       %Eta HCE = HCEdues *…
                                BelShad*…EnvTrans * HCE abs * HCEEmics

    SolarAvailability=0.99;

      %Coefficients for receiver heat loss

        A0=-9.463;
        A1=3.030e-1;
        A2=-1.387e-3;
        A3=6.929e-6;
        B0=7.650e-2;
        B1=1.129e-7;


  %Heat Exchanger Parameters

      UA_SH=298000;
      UA_SG=2051000;
      UA_pre = 752000;

  %Storage Parameters

      TankAreaC = 2121.67;
      TankAreaH = TankAreaC;
      MassStorageC_initial = 3265;
      Q_ColdTank_initial = 2846555093;
      T_ColdTank_initial = 293;
      MassStorageH_initial = 0;
      Q_HotTank_initial = 0;
      T_HotTank_initial = 0;

for i=1:8760

  %Solar Field inlet temperature

  if i==1
      T_f_i(i,1)=297;
  else
      T_f_i(i,1)=T_o_out(i-1);
  end

  %Weather Reader -- Reads weather and serves as Solar Field part I
```

```
[Q_abs(i,1)] = WeatherReader(Long_St,Long_L,phi,L_spacing,
W_SCA,FocalLength,L_SCA_loop,L_SCA,etaField,
etaHCE,SolarAvailability,SolarArea,Day(i), Hour(i), DNI(i), Tamb(i),
WindSpeed(i),i);

   %Solar Field Calculations

   if Q_abs(i)<=0
      mdot_field(i,1)=0;
      Qdot_collected(i,1)=0;
      Qdot_collected_MW(i,1)=0;
      Qdot_absorbed_MW(i,1)=0;
   else
    [mdot_field(i,1), Qdot_collected(i,1), Qdot_collected_MW(i,1),
    Qdot_absorbed_MW(i,1)] = SolarField…
    (T_f_i(i),T_f_o,A0,A1,A2,A3,B0,B1,DNI(i),Tamb(i),Q_abs(i),SolarArea,…
    h_field_out );
   end

   %Solar Field cumulative values

   FieldRatio(i,1)=mdot_field(i)/mdotField_ref;
   Q_Total_Incidence_MW(i,1)=DNI(i)*SolarArea/1000000;

   %Initiate Thermal Storage

   if i ==1

      MassStorageC(i,1) = MassStorageC_initial;
      Q_ColdTank(i,1) = Q_ColdTank_initial;
      T_ColdTank(i,1) = T_ColdTank_initial;
      MassStorageH(i,1) = 0;
      Q_HotTank(i,1) = 0;
      T_HotTank(i,1) = 0;

   else

      MassStorageC(i,1) = MassStorageC(i-1);
      Q_ColdTank(i,1) = Q_ColdTank(i-1);
      T_ColdTank(i,1) = T_ColdTank(i-1);
      MassStorageH(i,1) = MassStorageH(i-1);
      Q_HotTank(i,1) = Q_HotTank(i-1);
      T_HotTank(i,1) = T_HotTank(i-1);

   end
```

```
[T_o_out(i,1),mdot_s(i,1), T_salt_to_PB(i,1), mdot_to_PB(i,1), T_HotTank(i,1),
MassStorageH(i,1),Q_HotTank(i,1),T_HotTank_toHX(i,1),dT(i,1)] =
StorageControlsSalt(mdot_field(i),T_ColdTank(i),TankAreaH, MassStorageH(i),
Q_HotTank(i), T_HotTank(i),MassStorageC(i));

    %Divide Field Flow into steam train and reheat

        mdot_h_sh(i,1) = 0.872*mdot_to_PB(i);
        mdot_h_rh(i,1) = 0.128*mdot_to_PB(i);

    %Turn power plant on if power is greater than 3 MW -->66kg/s Field Flow

    if mdot_to_PB(i)<66
        T2(i,1)=0;
        T3(i,1)=0;
        T4(i,1)=0;
        T5(i,1)=0;
        T6(i,1)=0;
        T8(i,1)=0;
        Qpre(i,1)=0;
        Qsh(i,1)=0;
        Qsg(i,1)=0;
        P(i,1)=0;
        mdot_w(i,1)=0;
        T_out_HP2(i,1)=0;
        h_out_HP2(i,1)=0;
        Pout_HP2(i,1)=0;
        T_w_rh_out(i,1)=0;
        T_htf_rh_out(i,1)=0;
        h_rh_diff(i,1)=0;
        W_HP1(i,1)=0;
        W_HP2(i,1)=0;
        W_LP1(i,1)=0;
        W_LP2(i,1)=0;
        W_LP3(i,1)=0;
        W_LP4(i,1)=0;
        W_LP5(i,1)=0;
        T_to_exp(i,1)=0;
        T_to_ColdTank(i,1)=0;
        mdot_to_ColdTank(i,1)=0;
    else

        %Heat Exchanger Steam Train

            [T2(i,1), T3(i,1), T5(i,1), T6(i,1), Qsh(i,1), Qsg(i,1), P(i,1), mdot_w(i,1)] =
…
```

```
    f_main_search_salt(T_salt_to_PB(i),mdot_h_sh(i),UA_SH, UA_SG);
     [T4(i,1), T8(i,1), Qpre(i,1)] = Preheater_salt(mdot_h_sh(i),mdot_w(i),…
     P(i),T3(i),T6(i));

  % Calculate turbine pressures from mass flow rate

     [Pout_LP5 Pout_LP4 Pout_LP3 Pout_LP2 Pin_LP1 Pout_LP1
Pout_HP2(i,1) Pin_HP1 Pout_HP1...
mdot_LP5,mdot_LP4,mdot_LP3,mdot_LP2,mdot_LP1,mdot_HP2,…
mdot_HP1]…= TurbinePressure (mdot_w(i),Tamb(i));

  % High Pressure Turbine

     [W_HP1(i,1) W_HP2(i,1) T_out_HP2(i,1) h_out_HP2(i,1)] =…
      Turbine_HP…
     (T5(i), Pin_HP1, Pout_HP1, mdot_HP2, mdot_HP1, Pout_HP2(i));

  % Reheater Calculations

     [T_htf_rh_out(i,1), T_w_rh_out(i,1)]= Reheater_salt(mdot_LP1,…
    Pout_HP2(i), T_salt_to_PB(i),mdot_h_rh(i),h_out_HP2(i));

  % Low Pressure Turbine
     [W_LP1(i,1) W_LP2(i,1) W_LP3(i,1) W_LP4(i,1) W_LP5(i,1)] =…
    Turbine_LP (T_w_rh_out(i), Pin_LP1, Pout_LP1, Pout_LP2, …
    Pout_LP3, Pout_LP4, Pout_LP5,
    mdot_LP5,mdot_LP4,mdot_LP3,mdot_LP2,mdot_LP1);
     %h_rh_diff(i,1) = h_out_HP2(i) - XSteam('h_px',Pout_HP2(i),1);

  % Salt Mixer
     [T_to_ColdTank(i,1),mdot_to_ColdTank(i,1)] = Mixer_salt…
    (mdot_h_sh(i), mdot_h_rh(i),T4(i),T_htf_rh_out(i));

end

%Mass and Energy Balance on Cold Tank


[Q_ColdTank(i,1),T_ColdTank_toHX(i,1),T_ColdTank(i,1),MassStorageC(i,1)]
= ColdTank2(TankAreaC, MassStorageC(i),Q_ColdTank(i), T_ColdTank(i),
mdot_to_ColdTank(i), mdot_s(i),T_to_ColdTank(i));

%Calculate Power

  [WelectricMW(i,1), Welectric(i,1)] = Generator(W_LP1(i), W_LP2(i),…
  W_LP3(i), W_LP4(i), W_LP5(i), W_HP1(i), W_HP2(i));
```

```
end

Storage_Mass_Balance =[MassStorageC+MassStorageH];
KeyParameters=[Q_Total_Incidence_MW,Qdot_absorbed_MW,Qdot_collected_
MW,WelectricMW,mdot_w,MassStorageH,T_HotTank,Q_HotTank,MassStorage
C,T_ColdTank,Q_ColdTank,mdot_to_PB,a];
xlswrite('Results_StoreSalt_4h_SM1_', KeyParameters, 'sheet1','A1');
```

```
function [T_o_out,mdot_s,
T_salt_to_PB,mdot_to_PB,T_HotTank,MassStorageH,…
Q_HotTank,T_HotTank_toHX,dT ] = StorageControlsSalt(mdot_field,…
T_ColdTank,TankAreaH, MassStorageH,Q_HotTank,
T_HotTank,MassStorageC)

% StorageControlSalt dictates how to charge, discharge, and dwell storage
tanks.
% JK 2009

% mdot_s exits MassStorageC
% mdot_to_PB goes to PB;

%Calculate salt flow rate from solar field ~ Field Flow

[T_o_out, mdot_s]= f_Storage_Charger_salt(mdot_field,T_ColdTank);
mdot_s = round(mdot_s);
T_salt_to_PB = 386;
mdot_o = mdot_field;

if mdot_s == 653
   mdot_s_in_H = 0;
   mdot_s_out_H = 0;
   mdot_to_PB = 653;
   [T_HotTank,MassStorageH,Q_HotTank,T_HotTank_toHX,dT] = HotTank…
   (TankAreaH, MassStorageH, Q_HotTank, T_HotTank, mdot_s_in_H,
mdot_s_out_H);

elseif mdot_s > 653

   %Does Cold Tank have enough to discharge entire flow?

   if MassStorageC >= mdot_s

      mdot_charge = mdot_s - 653;
      mdot_to_PB = 653;
```

```
        mdot_s_in_H = mdot_charge;
        mdot_s_out_H = 0;
        [T_HotTank,MassStorageH,Q_HotTank,T_HotTank_toHX,dT] = HotTank…
       (TankAreaH, MassStorageH, Q_HotTank, T_HotTank, mdot_s_in_H,…
       mdot_s_out_H);

    else

        mdot_charge = MassStorageC - 653;
        mdot_to_PB = 653;
        mdot_s = MassStorageC;
        T_salt_in=T_ColdTank;
        [T_o_out mdot_o] = f_Storage_Charger_salt2oil(mdot_s,T_salt_in);
        mdot_s_in_H = mdot_charge;
        mdot_s_out_H = 0;
        [T_HotTank,MassStorageH,Q_HotTank,T_HotTank_toHX,dT] = HotTank…
       (TankAreaH, MassStorageH, Q_HotTank, T_HotTank, mdot_s_in_H,…
       mdot_s_out_H);
     end

else

     if MassStorageH <=0

       if mdot_s <= 66

           mdot_charge = mdot_s;
           mdot_s_in_H = mdot_charge;
           mdot_s_out_H = 0;
           mdot_to_PB = 0;
           [T_HotTank,MassStorageH,Q_HotTank,T_HotTank_toHX,dT] =
HotTank…
          (TankAreaH, MassStorageH, Q_HotTank, T_HotTank, mdot_s_in_H,…
          mdot_s_out_H);

       else
           mdot_to_PB = mdot_s;
           mdot_s_in_H = 0;
           mdot_s_out_H = 0;
           [T_HotTank,MassStorageH,Q_HotTank,T_HotTank_toHX,dT] =
HotTank…
          (TankAreaH, MassStorageH, Q_HotTank, T_HotTank, mdot_s_in_H,…
          mdot_s_out_H);
       end

    else
```

```
        mdot_needed = 653 - mdot_s;

        if MassStorageH == mdot_needed

           mdot_discharge = mdot_needed;
           mdot_s_in_H = 0;
           mdot_s_out_H = mdot_discharge;
           [T_HotTank,MassStorageH,Q_HotTank,T_HotTank_toHX,dT] =
HotTank…
          (TankAreaH, MassStorageH, Q_HotTank, T_HotTank, mdot_s_in_H,…
           mdot_s_out_H);
           %mix field plus storage
           [T_salt_to_PB,mdot_to_PB] = Mixer_salt2(mdot_s,mdot_discharge,…
          T_HotTank_toHX);

        elseif MassStorageH > mdot_needed
           mdot_discharge = mdot_needed;
           mdot_s_in_H = 0;
           mdot_s_out_H = mdot_discharge;
           [T_HotTank,MassStorageH,Q_HotTank,T_HotTank_toHX,dT] =
HotTank…
          (TankAreaH, MassStorageH, Q_HotTank, T_HotTank, mdot_s_in_H,…
          mdot_s_out_H);
           %mix field plus storage
           [T_salt_to_PB,mdot_to_PB] = Mixer_salt2(mdot_s,mdot_discharge,…
          T_HotTank_toHX);
        else
           mdot_capable = MassStorageH + mdot_s;

           if mdot_capable >= 66

              mdot_discharge = MassStorageH;
              mdot_s_in_H = 0;
              mdot_s_out_H = mdot_discharge;
              [T_HotTank,MassStorageH,Q_HotTank,T_HotTank_toHX,dT] =
HotTank…
             (TankAreaH, MassStorageH, Q_HotTank, T_HotTank, mdot_s_in_H,…
             mdot_s_out_H);
              %mix field plus storage
              [T_salt_to_PB,mdot_to_PB] = Mixer_salt2(mdot_s,mdot_discharge,…
             T_HotTank_toHX);
           else
              mdot_charge = mdot_s;
              mdot_s_in_H = mdot_charge;
              mdot_s_out_H = 0;
```

```
            [T_HotTank,MassStorageH,Q_HotTank,T_HotTank_toHX,dT] =
HotTank (TankAreaH, MassStorageH, Q_HotTank, T_HotTank, mdot_s_in_H,
mdot_s_out_H);
            %mix field plus storage
            mdot_to_PB = 0;
          end
        end
    end
end
```

```
function [T_o_out mdot_s] = f_Storage_Charger_salt(mdot_surplus,T_salt_in)

% f_Storage_Charger_salt calls the optimization routine Oil-Salt HX
% JK 2009

mdot_o = mdot_surplus;
if mdot_o < 4
   mdot_s = mdot_o*1.6;
   if mdot_s ==0
   T_o_out = 0;
   else
   %oil temp is
   T_o_out = 390.56 - mdot_s*(1443 + 0.172 * 339.5)*(386-T_salt_in)/(mdot_o*…
   1000*(1.509 + 0.002496 * 330.56 + 0.0000007888 * 330.56^2));
   end

else

UA_OtoS = 14063000;

%This function calls the optimization for the charger

warning off
%options =
optimset('LargeScale','on','Display','iter','TolX',.0000005,'TolFun',.00001,…
'MaxIter',10^6,'MaxFunEval',10^6);

options =
optimset('LargeScale','on','Display','off','TolX',.00000001,'TolFun',.0000005,…
'MaxIter',10^6,'MaxFunEval',10^6);

X=[mdot_o UA_OtoS,T_salt_in];

%call optimiztion routine
```

```
[mdot_s,Q_diff]=fminsearch(@Storage_Charger,mdot_o*1.6,options,X);

[Q_diff Sol]=Storage_Charger(mdot_s,X);

T_o_out=Sol(1);  Q_o=Sol(2);  Q_salt_in=Sol(3); mdot_s=Sol(4); eps=Sol(5);

end
```

```
function [Q_diff,Sol]=Storage_Charger(mdot_s,X)

% Storage_Charger converges energy balance and eps-NTU
% JK 2009

mdot_o=X(1);
UA_OtoS=X(2);
T4=X(3);

X=[mdot_o UA_OtoS,T4];

T1=393;
T3=386;
dh_salt = 1443 * (T3-T4) + 0.086 * (T3-T4)^2;       %[J/kg]


cps = 1443 + 0.172 * 339.5;
cpo=1000 * (1.509 + 0.002496 * (T1-60) + 0.0000007888 * (T1-60)^2);


%_____________________________________________________Oil to Salt

Cmin = min(cpo*mdot_o,cps*mdot_s);
Cmax = max(cpo*mdot_o,cps*mdot_s);
Cr = Cmin/Cmax;
UA_OtoS = UA_OtoS*(mdot_o/396)^0.8;
NTU=UA_OtoS/Cmin;

eps=(1-exp(NTU*(Cr-1)))/(1-Cr*exp(NTU*(Cr-1)));
Q = Cmin*eps*(T1-T4);

T_o_out=T1-((mdot_s*dh_salt*1.03)/(mdot_o*cpo));

Q1=mdot_o*cpo*(T1-T_o_out);

Q_diff=abs(Q-Q1);
Q_salt_in = Q1/1.03;
```

```
Sol=[T_o_out Q Q_salt_in mdot_s eps];
```

```
function [T_HotTank,MassStorageH,Q_HotTank,T_HotTank_toHX,dT] =
HotTank(TankAreaH, MassStorageH,Q_HotTank, T_HotTank, mdot_s_in_H,
mdot_s_out_H)

%Hot Tank calculates the temperature, mass, and energy in the hot storage tank
%JK 2009

%Assumptions
%cp stays constant
%Heat loss is f(TankArea) not f(TankArea,T_Tank)

dMstorage_in = mdot_s_in_H;                    %[kg]
dMstorage_out = mdot_s_out_H;
T_last = T_HotTank;
T_in =386+273;                          %[K]

if Q_HotTank ==0
   T_last = T_in;
else
   T_last = T_last+273;
end

Q_loss = 68 * TankAreaH;                    %[W]
MassStorageH = MassStorageH + dMstorage_in - dMstorage_out;
cp = 1443 + 0.172*(380+273);                %[J/kgK]
Q_in = dMstorage_in*cp*T_in;                %[J]
Q_out = dMstorage_out*cp*T_last;            %Tank_Last
Q_tank = Q_HotTank+Q_in-Q_out;              %[J]

if MassStorageH == 0
   T_tank = 0;
   dT = 0;
else
   T_tank = Q_tank/(MassStorageH*cp);
   dT = Q_loss/(MassStorageH*cp);
end


if MassStorageH <=0
   if dMstorage_out>0
      T_HotTank_toHX =T_last-273;
```

```
        T_HotTank = 0;
        Q_HotTank = 0;
    else
        T_HotTank = 0;
        Q_HotTank = 0;
        T_HotTank_toHX = 0 ;
        Percent_loss = 0;
    end
else
    T_HotTank = T_tank - dT-273;
    Q_HotTank = Q_tank - Q_loss;
    T_HotTank_toHX = T_last-273;
    Percent_loss = Q_loss/Q_tank;
end
```

```
function [Pout_LP5 Pout_LP4 Pout_LP3 Pout_LP2 Pin_LP1 Pout_LP1
Pout_HP2 Pin_HP1 Pout_HP1...
 %
mdot_LP5,mdot_LP4,mdot_LP3,mdot_LP2,mdot_LP1,mdot_HP2,mdot_HP1] =
TurbinePressure (mdot_w,Tamb)

    %mdot_w = 38.8;
    %Tamb = 20;
    %This function returns the mass flow rates and pressures for the turbine
stages
    Pin_HP1_ref = 100;
    Pout_HP1_ref = 33.61;
    Pin_HP2_ref = 33.61;
    Pout_HP2_ref = 18.58;
    %Pressure drop from High Pressure out to Low Pressure in
    Pin_LP1_ref = 17.10;
    Pout_LP1_ref = 7.98;
    Pin_LP2_ref = Pout_LP1_ref;
    Pout_LP2_ref = 2.73;
    Pin_LP3_ref = Pout_LP2_ref;
    Pout_LP3_ref = 0.96;
    Pin_LP4_ref = Pout_LP3_ref;
    Pout_LP4_ref = 0.29;
    Pin_LP5_ref = Pout_LP4_ref;
    Pout_LP5_ref = 0.08;
    mdot_LP5_ref=0.689*38.8;
    mdot_LP4_ref=0.709*38.8;
    mdot_LP3_ref=0.751*38.8;
    mdot_LP2_ref=0.797*38.8;
    mdot_LP1_ref=0.849*38.8;
```

```
    mdot_HP2_ref=0.925*38.8;
    mdot_HP1_ref=38.8;


    mdot_LP5=0.689*mdot_w;
    mdot_LP4=0.709*mdot_w;
    mdot_LP3=0.751*mdot_w;
    mdot_LP2=0.797*mdot_w;
    mdot_LP1=0.849*mdot_w;
    mdot_HP2=0.925*mdot_w;
    mdot_HP1=mdot_w;

    %Pressure at lowest turbine exit is function of condensing pressure,
    %Psat@Tamb
    Pout_LP5=XSteam('psat_T',Tamb+7);

    Pin_LP5=((mdot_LP5/mdot_LP5_ref)^2*(Pin_LP5_ref^2-
    Pout_LP5_ref^2)+Pout_LP5^2)^0.5;
    Pout_LP4=Pin_LP5;
    Pin_LP4=((mdot_LP4/mdot_LP4_ref)^2*(Pin_LP4_ref^2-
          Pout_LP4_ref^2)+Pout_LP4^2)^0.5;
    Pout_LP3=Pin_LP4;
    Pin_LP3=((mdot_LP3/mdot_LP3_ref)^2*(Pin_LP3_ref^2-…
     Pout_LP3_ref^2)+Pout_LP3^2)^0.5;
    Pout_LP2=Pin_LP3;
    Pin_LP2=((mdot_LP2/mdot_LP2_ref)^2*(Pin_LP2_ref^2-
Pout_LP2_ref^2)+Pout_LP2^2)^0.5;
    Pout_LP1=Pin_LP2;
    Pin_LP1=((mdot_LP1/mdot_LP1_ref)^2*(Pin_LP1_ref^2-
Pout_LP1_ref^2)+Pout_LP1^2)^0.5;
    %Can make a correction for pressure loss in the reheater stage
    Pout_HP2=Pin_LP1;
    Pin_HP2=((mdot_HP2/mdot_HP2_ref)^2*(Pin_HP2_ref^2-
Pout_HP2_ref^2)+Pout_HP2^2)^0.5;
    Pout_HP1=Pin_HP2;
    Pin_HP1=((mdot_HP1/mdot_HP1_ref)^2*(Pin_HP1_ref^2-
Pout_HP1_ref^2)+Pout_HP1^2)^0.5;
```

REFERENCES

[1] http://www.flagsol.com/SEGS_tech.htm

[2] www.nevadasolarone.net

[3] Winter, C.J., et al., 1991, “Solar Power Plants,” Springer-Verlag, Berlin, Heidelber.

[4] Relloso, Sergio, et al., 2008 “Real Application of Molten Salt Thermal Storage to Obtain High Capacity Factors in Parabolic Trough Plants,” 42709_1i_5, SolarPACES, Las Vegas, NV.

[5] Kutscher, Charles F., “Tackling Climate Change in the U.S.”, American Solar Energy Society, January 2007

[6] Hermann, Ulf, Kearney D., “Survey of Thermal Energy Storage for Parabolic Trough Power Plants,” Journal of Solar Energy Engineering, Vol. 124, pp145-152.

[7] Price, H., 2003 “A Parabolic Trough Solar Power Plant Simulation Model,” International Solar Energy Conference, Hawaii Island, Hawaii.

[8] Lippke, Frank, 1995, “Simulation of the Part-Load Behavior of a 30 MWe SEGS Plant,” SAND95-1293, Sandia National Laboratories, Albuquerque, NM.

[9] Solar Advisor Model (SAM), 2006, National Renewable energy Laboratory, Golden CO.

[10] Patnode, Angela, 2006, “Simulation and Performance Evaluation of Parabolic Trough Solar Power Plants,” Thesis, University of Wisconsin, Madison.

[11] Herrmann, Ulf, et al. 2002, “Overview on Thermal Storage Systems,” Flabeg Solar International GmbH, Workshop on Thermal Storage for Trough Power Systems.

[12] Nexant Inc., “USA Trough Initiative Nitrate Salt Heat Transport Fluid: Rankine Cycle, Steam Generator, and Thermal Storage Analyses.” January 19, 2001

[13] Schulte-Fischedick, Jan, et al., 2008, “CFD Analysis of the Cool Down Behaviour of Molten Salt Thermal Storage Systems,” ASME, Proceedings of ES2008, Jacksonville, FL.

[14] Kearney, D., et al., 2002, “Evaluation of a Molten Salt Heat Transfer Fluid in a Parabolic Trough Solar Field,” ASME International Solar Energy Conference, Reno, NV.

[15] Incropera, Frank P. and Dewitt, David, “Fundamentals of Heat and Mass Transfer. 4th Edition. New York: John Wiley and Sons, Inc. 2002.

[16] Duffie, John, and Beckman William, “Solar Engineering of Thermal Processes”, John Wiley & Sons Inc., New Jersey, 2006.

[17] Shah, Ramesh K. and Sekulic, Dusan P., “Fundamentals of Heat Exchanger Design”, John Wiley & Sons Inc., New Jersey, 2003.

[18] Nexant Inc., 2001, “Thermal Storage Oil-to-Salt Heat Exchanger Design and Safety Analysis,” Task Order Authorization Number KAF-9-29765-09, San Francisco, CA.

[19] Kopp, Joseph and R.F. Boehm, “Comparison of Two-Tank Indirect Thermal Storage Designs for Solar Parabolic Trough Power Plants,” ASME, Proceedings of ES2009, San Francisco, CA.

VITA

Graduate College
University of Nevada, Las Vegas

Joseph Kopp

Local Address:
4051 Brighthill Ave
Las Vegas, NV 89121

Degrees:
Bachelor of Arts, Physics, 2004
Lewis & Clark College

Publications:

Joseph Kopp, R.F. Boehm. “Comparison of Two-Tank Indirect Thermal Storage Designs for Solar Parabolic Trough Power Plants,” Proceedings of ES2009, Energy Sustainability 2009, July 19-13, San Francisco, CA

R. Cabanillas, J. Kopp. "Measuring Energy Efficiency from a 4kW Dish Concentrator System Using Older Parabolic Antenna Technology," International Solar Energy Society-Solar World Congress Proceedings, September 18-21, 2007, Beijing, China

Thesis Title: Two-Tank Indirect Thermal Storage Designs for Solar Parabolic Trough Power Plants

Thesis Examination Committee:
Chairperson, Robert Boehm, Ph. D.
Committee Member, Yitung Chen, Ph. D
Committee Member. Dan Cook, Ph. D.
Graduate College Representative, Yahia Baghzouz, Ph. D.